AGU PUBLICATIONS

JGR

Journal of Geophysical Research: Oceans

RESEARCH ARTICLE

10.1002/2016JC011959

New insights on the upper layer circulation north of the Gulf of Guinea

G. Herbert[1], B. Bourlès[1], P. Penven[2], and J. Grelet[3]

[1]Institut de Recherche pour le Développement, Laboratoire d'Etudes en Géophysique et Océanographie Spatiales, Brest, France, [2]Institut de Recherche pour le Développement, Laboratoire d'Océanographie Physique et Spatiale, Brest, France, [3]Institut de Recherche pour le Développement, Unité de Service Instrumentation, Moyens Analytiques, Observatoires en Géophysique et Océanographie, Brest, France

Key Points:
- A 100/250 m depth eastward current observed north of 4°N in the Gulf of Guinea: the Guinea UnderCurrent
- The Guinea UnderCurrent is stronger in spring and reverses westward in August–September
- It is fed from recirculation current system and a weak subsurface current flowing along the West African coast

Correspondence to:
G. Herbert,
gaelle.herbert@ird.fr

Citation:
Herbert, G., B. Bourlès, P. Penven, and J. Grelet (2016), New insights on the upper layer circulation north of the Gulf of Guinea, *J. Geophys. Res. Oceans*, *121*, 6793–6815, doi:10.1002/2016JC011959.

Received 11 MAY 2016
Accepted 26 AUG 2016
Accepted article online 29 AUG 2016
Published online 13 SEP 2016

Abstract The oceanic circulation in the upper layers of the north of the Gulf of Guinea is analyzed, as inferred from in situ observations and numerical simulations. This particular region, in spite of the presence of a coastal upwelling and its impact on resources and regional climate, is still poorly documented. Cruises carried out in the framework of different international programs (e.g., EGEE/AMMA, PIRATA) allowed to show the existence of an eastward flowing undercurrent, found under the Guinea Current, named the Guinea UnderCurrent (GUC). Numerical results from high resolution simulation allowed the description of the seasonal variability of this current. It appears that the GUC is stronger in spring and reverses westward in August–September. We also depict the fate and the sources of the GUC based on selected trajectories from numerical particle tracking. The simulated trajectories reveal: (i) a preferred route of the GUC along 4°N from Cape Palmas to Cape Three Points and following the coast east of Cape Three Points; (ii) strong recirculations in the most eastern part of the Gulf of Guinea and off Cape Palmas including warm and salty waters of the South Equatorial Current; (iii) a weak inflow from northern latitudes through a subsurface current flowing southward along the West African coast. In addition, Lagrangian experiments show that the GUC is not an extension of the North Equatorial UnderCurrent and confirm that this current does not penetrate into the Gulf of Guinea.

1. Introduction

The Gulf of Guinea (GG) is a particular region of the Tropical Atlantic characterized by a strong variability of the Sea Surface Temperature (SST) at seasonal to interannual time scales [e.g., *Picaut*, 1983], and where the Equatorial UnderCurrent (EUC) termination plays a significant role for the Atlantic Subtropical Cell and the global inter-hemispheric transport of salty subtropical waters [e.g., *Hazeleger and de Vries*, 2003; *Schott et al*., 2004]. It has been the subject of many recent studies, mainly dedicated to the analysis of the processes responsible for the Atlantic Cold Tongue (ACT) and its potential impact on the West African Monsoon (WAM) in the framework of the international "African Monsoon Multidisciplinary Analysis" (AMMA) [*Redelsperger et al*., 2006] program [e.g., *Kolodziejczyk et al*., 2009; *Marin et al*., 2009; *Brandt et al*., 2011; *Caniaux et al*., 2011; *Leduc-Leballeur et al*., 2013].

The GG is also a place where a particular coastal upwelling is present in the North along the zonal coast between Liberia and Nigeria [*Roy*, 1995]. In contrast to other most coastal upwelling systems, it occurs along a zonal coast and is not explained by the wind and Ekman theory only [*Bakun*, 1978]. Different hypothesis have been put forward [*Marchal and Picaut*, 1977; *Djakouré et al*., 2014, 2016] to explain this upwelling, including the seasonal intensification of the Guinea Current (GC) [*Morlière*, 1970; *Bakun*, 1978; *Colin*, 1988].

The GC is generally considered as an eastward continuation of the North Equatorial CounterCurrent (NECC), intensified in boreal summer-fall [*Hisard and Merle*, 1979; *Arnault*, 1987; *Stramma and Schott*, 1999; *Lumpkin and Garzoli*, 2005]. However, a precise description of the circulation in the north of Gulf of Guinea and of its variability is still needed for a better understanding of the regional ocean and coastal upwelling dynamics. Close to the coast, a westward current under the GC were measured for the first time in September 1964 and described by *Donguy and Privé* [1964], firstly named Guinea CounterCurrent (GCC) or Ivoirian UnderCurrent (IUC) for its component located over the continental shelf [*Lemasson and Rebert*, 1968], then Guinea

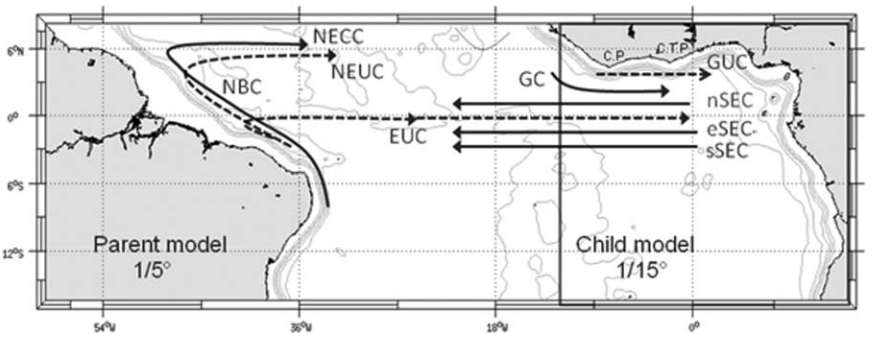

Figure 1. Parent and child 's domain (indicated by the black square) superimposed with black solid and dashed arrows indicating respectively main surface and subsurface currents in the area: NEC: North Equatorial Current; nSEC: Northern South Equatorial Current, cSEC: Central South Equatorial Current; sSEC: Southern South Equatorial Current; EUC: Equatorial Under Current; NECC: North Equatorial Counter Current; NEUC: North Equatorial Under Current; NBC: North Brazil Current; GC: Guinea Current; GUC: Guinea Under Current. The contours lines indicate the bathymetry at 1000, 1500, 2000, 3000, and 4000 m. Cape Palmas and Cape Three Points are respectively indicated by *C.P* and *C.T.P*.

UnderCurrent (GUC) by *Lemasson and Rebert* [1973a]. *Lemasson and Rebert* [1973b] suggested that the GUC originates in the far east of the Gulf of Guinea and appears at the surface during some periods of the year, and named the westward flow observed around 3°N west of 6°E the GCC. *Verstraete* [1992] described the subthermocline westward flows as being separated in two components: a coastal GUC flowing along the shelf break and, around 3°N, the GCC considered as being a possible northern part of the EUC return flow. At subsurface depths, the fate of the eastward North Equatorial UnderCurrent (NEUC) in the eastern Tropical Atlantic is still not clear. This current, fed by subtropical salty waters, also contributes to the Subtropical Cell and supplies upwelled waters in the East. Most of the studies suggest that the NEUC does not penetrate into the GG, since it is rather deviated northward during its eastward route off West Africa and veering within the Guinea Dome [*Hisard et al*., 1976; *Arhan et al*., 1998; *Stramma and Schott*, 1999; *Bourlès et al*., 2002]. However, *Mercier et al*. [2003] observed subsurface eastward currents in January–March 1995 (i) at 9°W around 2° 30′N that they suggested to be a signature of the NEUC and (ii) at 3°E around 4°N that they attributed to the GC (and not to the NEUC). During the same period, these authors also observed a westward flow associated with salinity maximum waters around 3°N at 3°E. Such subsurface salinity maximum, that can only be transported by the EUC into the region, has already been observed either associated to westward or eastward flows [e.g., *Piton and Wacongne*, 1985; *Verstraete;* 1992; *Gouriou and Reverdin*, 1992]. From recent in situ measurements, *Kolodziejczyk et al*. [2014] clearly evidenced EUC westward recirculations in the eastern GG south and north of the equator, around 3°S and 3°N, confirming earlier suggestions by *Verstraete* [1992], but additionally described the seasonal variability of these currents and of the EUC maximum salinity waters fate in the equatorial band. The northern recirculation around 3°N could correspond to the GCC described by *Lemasson and Rebert* [1973b] and *Verstraete* [1992] at this latitude, but could also be associated with the northern branch of the South Equatorial Current (nSEC) [*Stramma and Schott*, 1999]. Precise definitions and descriptions of both the GCC and the GUC and of their variability are still missing and are needed.

In this paper, we provide additional information of the currents in the north of the Gulf of Guinea as inferred from in situ observations carried out in the framework of different international programs, and mostly focus on eastward flows. The analysis of observations clearly evidences the presence of an eastward flow with relative velocity maxima in the 100/250 m depth range close to the coast, which may reverse to a westward flow. Hereinafter, and to clarify the different currents names found in the literature, we will define this flow to be the Guinea UnderCurrent (GUC) since it is observed below the GC and in the same direction. The detailed analysis of our observations induce some questions: 1) is the GUC the result of a direct advection from the west or of local recirculation? 2) what is its seasonal variability? 3) is it linked to the GC, part of it, or the signature of local circulation pattern?

Since the cruises are sparsely distributed along the year, we also use results of a high resolution numerical model of the regional ocean circulation in order to better describe the complex circulation in this particular area and to analyze the seasonal variability of the observed currents (Figure 1). In particular, our

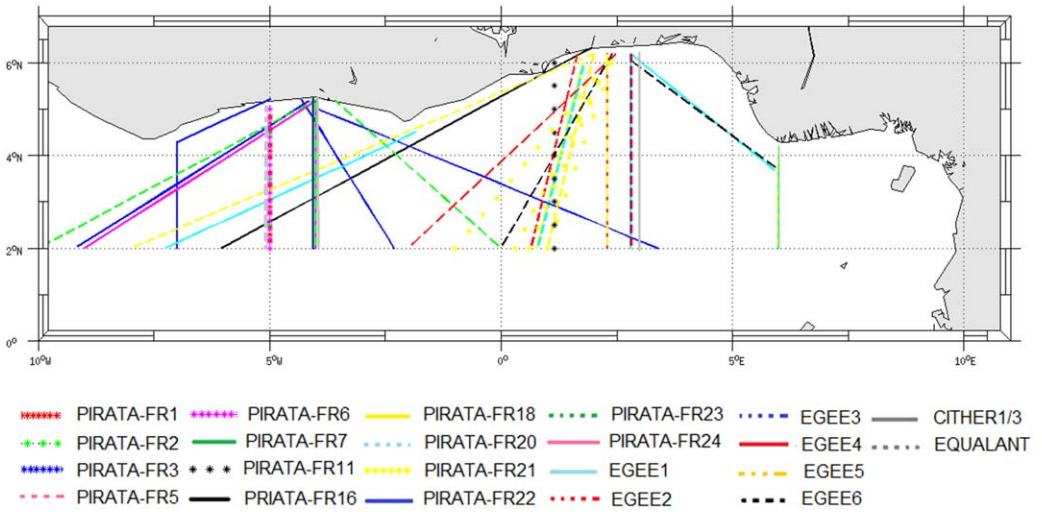

Figure 2. Map of oceanographic sections obtained during EQUALANT, PIRATA, EGEE, and CITHER1/3 cruises.

investigation takes a Lagrangian point of view based on a tracking of particles advected by the model velocity field in order to further clarify the water mass pathways in the studied region. The data, the numerical model and the Lagrangian tool are presented in section 2. Section 3 is dedicated to the description of in situ measurements while the model results are presented in section 4. After comparisons between the numerical model results and in situ measurements, the model is used to describe the seasonal variations of the currents and associated salinity. Then, the results obtained from Lagrangian experiments are described. Finally, a conclusive discussion of the main results is proposed in section 5.

2. Method

2.1. In Situ Data

The data used in this study were collected in the Gulf of Guinea principally during recent cruises carried out in the framework of the programs "Prediction and Research moored Array in the Tropical Atlantic" (PIRATA) [*Bourlès et al*., 2008] and « Etude de la circulation océanique et des échanges océan-atmosphère dans le Golfe de Guinée » (EGEE) [*Bourlès et al*., 2007], the French oceanographic component of the "African Monsoon Multidisciplinary Analysis" program (AMMA) [*Redelsperger et al*., 2006]. We also occasionally used additional older data from the CITHER-3 cruise [*Mercier et al*., 2003] and from the EQUALANT 1999 and 2000 cruises [*Bourlès et al*., 2002]. The data from cruise dates prior to 1995 have not been used due to a lack of precision of the current measurements. All the sections of the cruises carried out in our area of study are shown on Figure 2. During all these cruises, hydrological profiles were carried out at a spatial resolution of 1/3° to 1/2° in latitude along meridional sections. We have selected the measurements in the region of the Gulf of Guinea, north of 2°N. Temperature, salinity and dissolved oxygen measurements were collected from CTD-O2 SeaBird probes [*Kolodziejczyk et al*., 2009], except for during CITHER-3 cruise during which a Neil-Brown Mark III CTD instrument was used [e.g., *Hisard and Hénin*, 1987; *Gouriou and Reverdin*, 1992; *Mercier et al*., 2003]. For most of the cruises, measurements of the two horizontal components of the currents were carried out with a Ship-mounted Acoustic Doppler Current Profilers (SADCP) (for details on acquisition and measurements accuracy, see *Kolodziejczyk et al*. [2009] and *Herbert et al*. [2015]). En-route SADCP measurements cover the depth range from about 20 m down to 200 m or 350 m, depending upon the SADCP acoustic signal frequency. Absolute referencing was provided by Global Positioning System (GPS) navigation.

2.2. Numerical Model

The numerical model used in this paper is the Regional Oceanic Modeling System (ROMS) [*Shchepetkin and McWilliams*, 2005]. ROMS is a three-dimensional free surface, split-explicit ocean model which solves the Navier-Stokes primitive equations following the Boussinesq and hydrostatic approximations. We used the

ROMS version developed at the Institut de Recherche pour le Développement (IRD) featuring a two-way nesting capability based on AGRIF (Adaptative Grid Refinement In Fortran) [*Debreu et al*., 2012]. The two-way capability allows interactions between a large-scale (parent) configuration at lower resolution and a regional (child) configuration at high resolution (see Figure 1). The ROMSTOOLS package [*Penven et al*., 2008] is used for the design of the configuration. The model configuration is built following the one performed by *Djakouré et al*. [2014] over the Tropical Atlantic. The large scale domain extends from 60°W to 15.3°E and from 17°S to 8°N and the nested high resolution zoom focuses between 17°S and 6.6°N and between 10°W and 14.1°E domain. This configuration allows for equatorial Kelvin waves induced by trade wind variations in the western part of the basin to propagate into the Gulf of Guinea and influence the coastal upwelling [*Servain et al*., 1982; *Picaut*, 1983]. The horizontal grid resolution is 1/5° (i.e., 22 km) for the Tropical Atlantic (parent) grid and 1/15° (i.e., 7 km) for the Gulf of Guinea (child) grid. This should allow an accurate resolution of the mesoscale dynamics since the first baroclinic Rossby radius of deformation ranges from 150 to 230 km in the region [*Chelton et al*., 1998]. The vertical coordinate is discretized into 45 sigma levels with vertical S-coordinate surface and bottom stretching parameters set to theta_s=6 and theta_b=0, to keep a sufficient resolution near the surface for an accurate resolution of the GC [*Haidvogel and Beckmann*, 1999]. The vertical S-coordinate Hc parameter, which gives approximately the transition depth between the horizontal surface levels and the bottom terrain following levels, is set to Hc=10 m. The GEBCO1 (Global Earth Bathymetric Chart of the Oceans) is used for the topography (www.gebco.net). The runoff forcing is provided from Dai and Trenberth's global monthly climatological run-off data set [*Dai and Trenberth*, 2002]. The rivers properties of salinity and temperature are prescribed as annual mean values. One river (Amazon) is prescribed in the parent model while five rivers, that correspond to the major rivers present in the region, are prescribed in the child model (Congo, Niger, Ogoou, Sanaga, Volta). At the surface, the model is forced with the surface heat and freshwater fluxes as well as monthly wind stress climatology derived from the Comprehensive Ocean Atmosphere Data Set (COADS) (horizontal resolution of 1°x1) [*Da Silva et al*., 1994]. Our model has three open boundaries (North, South, and West) forced by temperature and salinity fields from the World Ocean Atlas 2009 (WOA09) monthly climatology (horizontal resolution of 1°x1°). The simulation has been performed on IFREMER Caparmor super-computer and integrated for 15 climatologic years with the outputs averaged every 2 days. A statistical equilibrium is reached after 6 years of spin-up. Model analyses are based on the monthly averaged model outputs averaged from year 7 to year 15.

2.3. The ARIANE Lagrangian Diagnostic Tool

Lagrangian diagnoses have been made using an off-line ARIANE Lagrangian diagnostic tool [*Blanke and Raynaud*, 1997, http://stockage.univ-brest.fr/grima/Ariane/] developed in LOPS (Laboratoire d'Océanographie Physique et Spatiale).

ARIANE is a computational tool dedicated to the offline computation of 3-D streamlines in a given output velocity field and subsequent water masses analyses. The analysis consists of releasing virtual particles and advecting them using the model 3-D time-varying velocity fields. As the particles are only advected by the model velocities fields, the turbulent diffusion processes are not explicitly used to calculate the trajectories. The signature of those processes, parameterized in the numerical model, is provided implicitly by the along-trajectory change in tracer properties calculated by the local Eulerian fields of the model. Otherwise, the diagnostic tool gives the possibility to choose between two different modes, qualitative and quantitative. For our study, Lagrangian experiments were performed offline to identify the pathway and the origin of the eastward subsurface current observed and simulated by the model north of 2°N. The trajectory of each particle is computed at every grid cell at their storage frequency, i.e., using successive monthly averaged modeled velocity fields. The method is presented in detail and discussed by *Blanke and Raynaud* [1997] and *Blanke et al*. [1999].

3. Results From In Situ Observations

All the six EGEE cruises carried out from 2005 to 2007 allowed to get high quality measurements along or around 2°50′E when leaving from, or returning back to, the port of Cotonou (Benin); three cruises were in early boreal summer (May–July) and the three other ones in boreal fall (September–November) during each

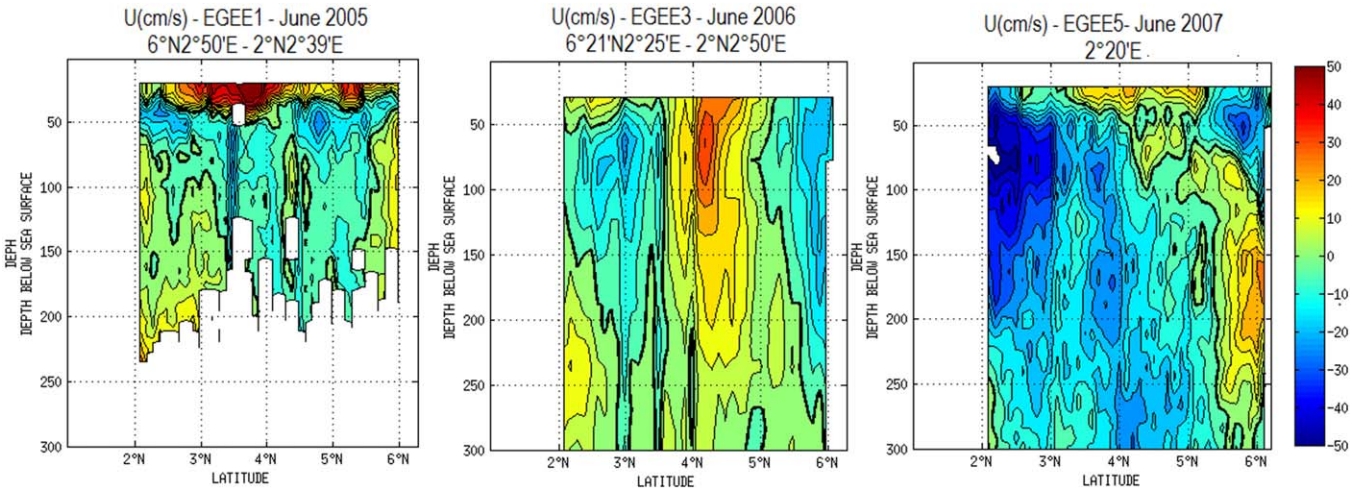

Figure 3. Vertical sections of zonal velocity (cm.s^{-1}) down to 300 meters depth from 2 min averaged SADCP measurements obtained during the EGEE1, EGEE3 and EGEE5 cruises, carried out respectively during 25–26 June 2005, 15–16 June 2006, and 14–16 June 2007 at 2°39′ E, 2°50′E and 2°20′E.

year. We mainly focus in this paper on the flows located north of 2–3°N, i.e., around the GC and surrounding flows.

3.1. Highlight of an Eastward Flow Below the GC

Measurements of the zonal component of the currents along 2°50′E and 2°20′E during the three cruises done in June (Figure 3) show the eastward GC in the upper 50 m between 2°30′N and 5°N in June 2005 and June 2007. In June 2006, it is mostly found between 3°30′N and 5°N. It appears with deeper extensions in June 2006 and 2007, when eastward velocities are observed down to 200/250 m depth below its surface velocity core (up to 20 cm.s^{-1}).

In June 2006 and June 2007, the GC is embedded between westward flows. The main one, located south of 4°N, corresponds to the GCC [*Lemasson and Rebert*, 1973b; *Verstraete*, 1992] and/or to the nSEC [*Tsuchiya*, 1986; *Stramma and Schott*, 1999]. The one observed close to the surface around and north of 5°N, with a relative velocity maximum around 50 m depth, corresponds to the GUC, according to *Lemasson and Rebert* [1973b]. This westward flow appears down to 250 m depth in June 2006, with a second relative velocity core around 150 m depth. In June 2005, the surface GC north-south extension is larger andthe distinction of the two westward flows is less evident.

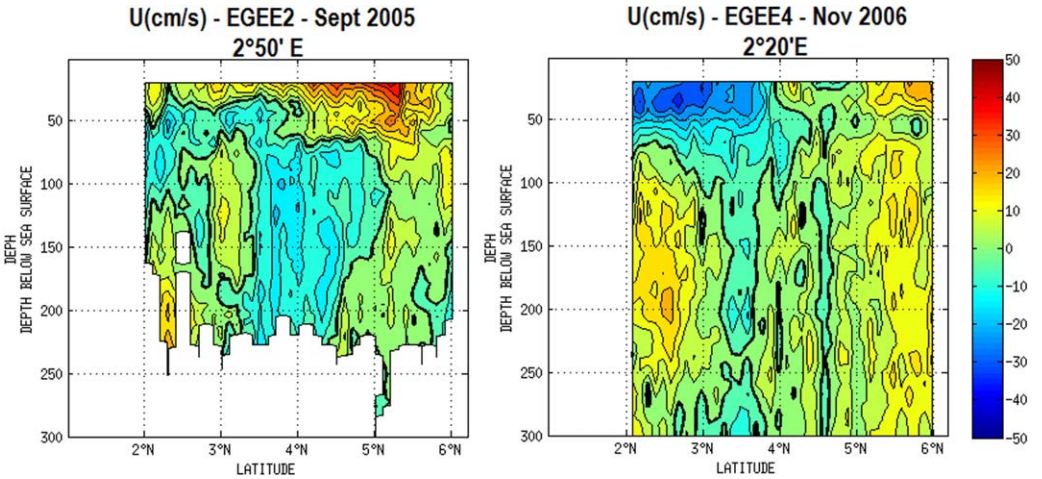

Figure 4. Vertical sections of zonal velocity (cm.s^{-1}) down to 300 m depth between 2°N and 6°N from 2 min averaged SADCP measurements obtained during the EGEE2 and EGEE4 cruises carried out respectively during (left) September 2005 at 2°50′E and (right) November 2006 at 2°20′E.

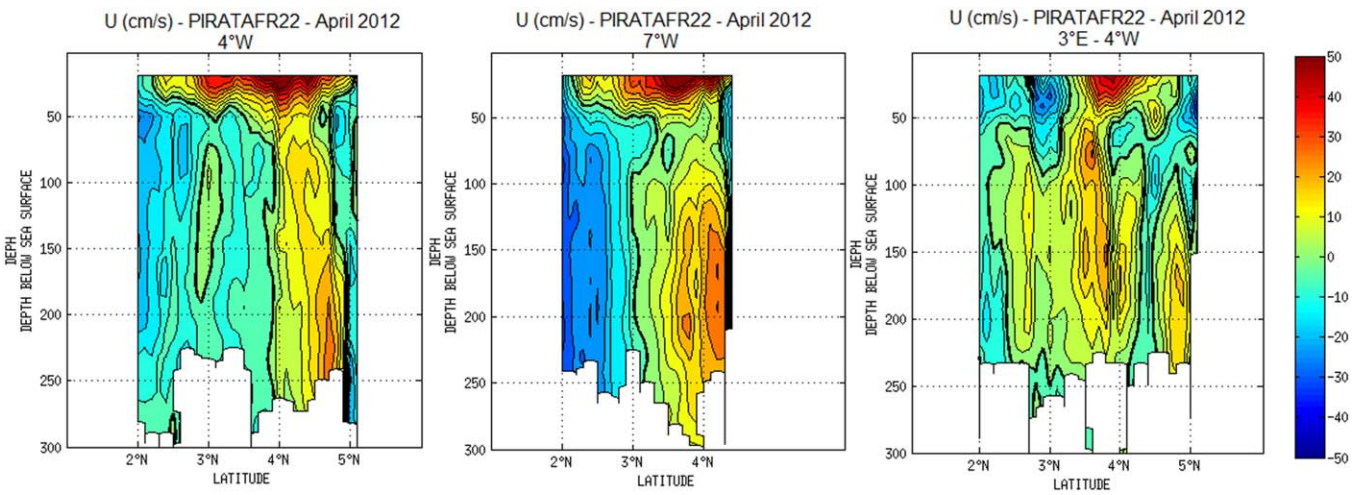

Figure 5. Vertical sections of zonal velocity (cm.s^{-1}) down to 300 meters depth north of 2°N from 2 min averaged SADCP measurement obtained during the PIRATA-FR22 cruise carried out in April 2012 respectively at (left) 4°W, (middle) 7°W, and (right) from 3°E/2°N to 4°W/5°N.

An interesting new feature is the presence of eastward flows trapped along the coast, with a velocity core between 50 and 150 m in June 2005 and between 150 and 200 m depth in June 2007, when eastward velocities reach 20 cm.s^{-1}. To our knowledge, it is the first time that such eastward flows, clearly distinct from the surface GC, are observed at this location (keeping in mind that this area was still very poorly documented before these cruises, principally below the surface).

In order to verify if such eastward subsurface coastal flows have also been observed at other longitudes and/or during other (previous) cruises, although they were not explicitly identified in the rare previous studies, we looked at other available zonal current sections that allowed evidencing the presence of these flows. For example, current measurements carried out in fall along the same longitude in September 2005 and November 2006 (Figure 4) also show the presence of a subsurface eastward velocity core trapped at the coast between 100 and 250 m depth in September and November 2006, but characterized with weaker velocities than during spring.

Farther in the west, measurements have been obtained along 4°W in April 2012 (PIRATA-FR22; Figure 5, left). During this cruise, the GC is observed between 2°30′N and 4°30′N with a velocity core about 30 m depth reaching 50 cm.s^{-1}. A westward flow is also observed from 4°30′N to the coast. A subsurface eastward flow is observed between 50 m to 250 m depth, below the GC, with a velocity maximum at 250 m depth (∼20 cm.s^{-1}) and between 4°N to 4°40′N. It is separated from the coast by a thin westward flow. Also along 4°W, a cruise done in October 1998 (PIRATA-FR2), strongly suggest the presence of a coastal eastward flow below 100 m depth (not shown).

The eastward current is also observed at 7°W, from measurements obtained in March 2012 (PIRATA-FR22; Figure 5, middle). At this location the GC extends from 2°N to 4°30′N with a surface velocity maximum of about 45 cm.s^{-1}. The eastward flow is observed below the GC from 100 m to 250 m depth with two maximum velocities: one close to the coast and another around 3°50′N. At this location, just off Cape Palmas, the eastward flow velocities are higher than farther in the east, suggesting two different contributions to this flow.

Along the slanted section from 3°E-2°N to 4°W-6°N (PIRATA-FR22; Figure 5, right), two eastward subsurface flows are observed: one branch between 3.5°N-4°N around 2°10′W and another branch trapped to the coast north of 5°N, between 3°10′W and 4°W.

In order to help the identification of the different observed currents, and to avoid any possible confusion due to the different names used in the literature for the same currents (as recalled in the introduction above), we choose hereinafter to name the coastal westward flow as the Guinea CounterCurrent (GCC, in opposite direction to the GC), and to name the eastward flow observed in the subsurface layers (same direction but at lower depths than the GC) the Guinea UnderCurrent (GUC), while the westward flow observe

Table 1. Observation of the GUC

Month	Year	Cruise	GUC (Y/N)	GUC Core Longitude	GUC Core Latitude	GUC Depth[a]
January	1995	Cither 3	Y	7°W	4°N	50–250 m
	1998	Pirata fr1b	Y	5°W	4°N	100–200 m
	1999	Pirata fr3	Y	5°W	4°N	150–200 m
	2003	Pirata fr11	Y	1°15′E	3°N	100–150 m
March	1993	Cither 1	Y	4°W	4°N	100–250 m
	1995	Cither 3	Y	3°E	4°N	100–250 m
	2000	Pirata fr6	Y	5°W	4°N	100–200 m
April	2012	Pirata fr22 leg1	Y	7°W	4°40′N	100–250 m
	2012	Pirata fr22 leg1	Y	5°10′W	4°30′N	100–250 m
	2012	Pirata fr22 leg2	Y	4°W	4°30′N	100–250 m
	2012	Pirata fr22 leg2	Y	6°W and 4°W	4°N and 4°48N	100–250 m and 150–250 m
	2012	Pirata fr22 leg3	Y	3°38′W	4°30N	100–250 m
	2012	Pirata fr22 leg3	Y	2°10′W and 3°10′W	4°N and 4.40°N	100–200 m and 150–250 m
	2014	Pirata fr24	Y	5°40′W	4°N	150–200 m
May	2011	Pirata fr21 leg1	Y	2°20′E	6°N	100–250 m
	2011	Pirata fr21 leg2	Y	2°20′E	6°N	100–200 m
	2011	Pirata fr21 leg2	Y	2°10′E	6°N	100–250 m
	2011	Pirata fr21 leg3	Y	2°25′E	5°50N	100–250 m
	2013	Pirata fr23 leg1	Y	5°40′W	4°N	150–250 m
	2014	Pirata fr24	Y	4°W	5°N	100–150 m
June	2005	Egee1	Y	6°E	3°N	100–200 m
	2005	Egee1	Y	2°50′E	5°30′N	50–200 m
	2005	Egee1	Y	2°W	4°N	50–200 m
	2005	Egee1	Y	2°50′E	6°N	50–100 m
	2006	Egee3	N	2°50′E		
	2007	Pirata fr16	Y	0°30′E	5°20′N	50–250 m
	2007	Egee5/Pirata fr17	Y	2°50′E	6°N	100–250 m
	2007	Egee5/Pirata fr17	Y	2°20′E	5°50′N	100–200 m
	2007	Egee5/Pirata fr17	Y	6°E	4°N	100–200 m
	2007	Egee5/Pirata fr17	Y	0°30′E	5°20′N	100–250 m
	2007	Egee5/Pirata fr17	Y	2°50′E	6°N	50–250 m
	2013	Pirata fr23 leg2	Y	2°30′W	4°N	150–250 m
	2013	Pirata fr23 leg2	Y	2°20′W	3°50′N	100–200 m
July	2000	Eq2000/Pirata fr7	N	6°E		
August	1999	Eq1999/Pirata fr5	N	5°W		
September	2005	Egee2	Y	2°50′E	5°30′N	50–150 m
	2005	Egee2	Y	2°20′E	5°N40′	50–150 m
	2005	Egee2	N	2°15′E		
	2007	Egee6	Y	1°45′E	5°20′N	50–250 m
	2008	Pirata fr18	Y	2°20′E	5°50′N	100–250 m
October	1998	Pirata fr2	Y	5°W	3°40′N	100–200 m
	2010	Pirata fr20 leg2	Y	1°53′E	5°N	50–200 m
November	2006	Egee4	Y	2°50′E	5°30′N	50–250 m

[a]Note that the depth range of the GUC is limited by the SADCP depth range (~200–300 m).

south of 4°N is clearly identified as to be a deep component of the nSEC, issued from the northern recirculation of the EUC. Analyzes of the SADCP zonal current measurements have been made for all the cruises at hand carried out in the area and the depth/latitude of the GUC during the different cruises has been identified and summarized in Table 1. In particular, we have selected 43 vertical sections located between 2°N and the northern coast and the Gulf of Guinea, sparsely distributed along the year (most of sections (26/43) are available during April/May/June while only 7 sections are available during boreal summer (July, August, September)).

The results indicate that:

1) the GUC is observed for all sections obtained during March/April/May and missing during those obtained during July/August where the current is reversed westward, suggesting a seasonal variability of the GUC; 2) When the GUC is observed, it is located around 4°N – 4°30′N in the western part of Gulf of Guinea and trapped to the coast in the eastern part of the Gulf; however for three sections obtained around 4°W, two veins are observed: one around 4°N-4°30′N and another one trapped to the coast; 3) The upper part of the GUC core tends to be deeper in winter and spring (from January to June) (150 m for 4/33 sections and

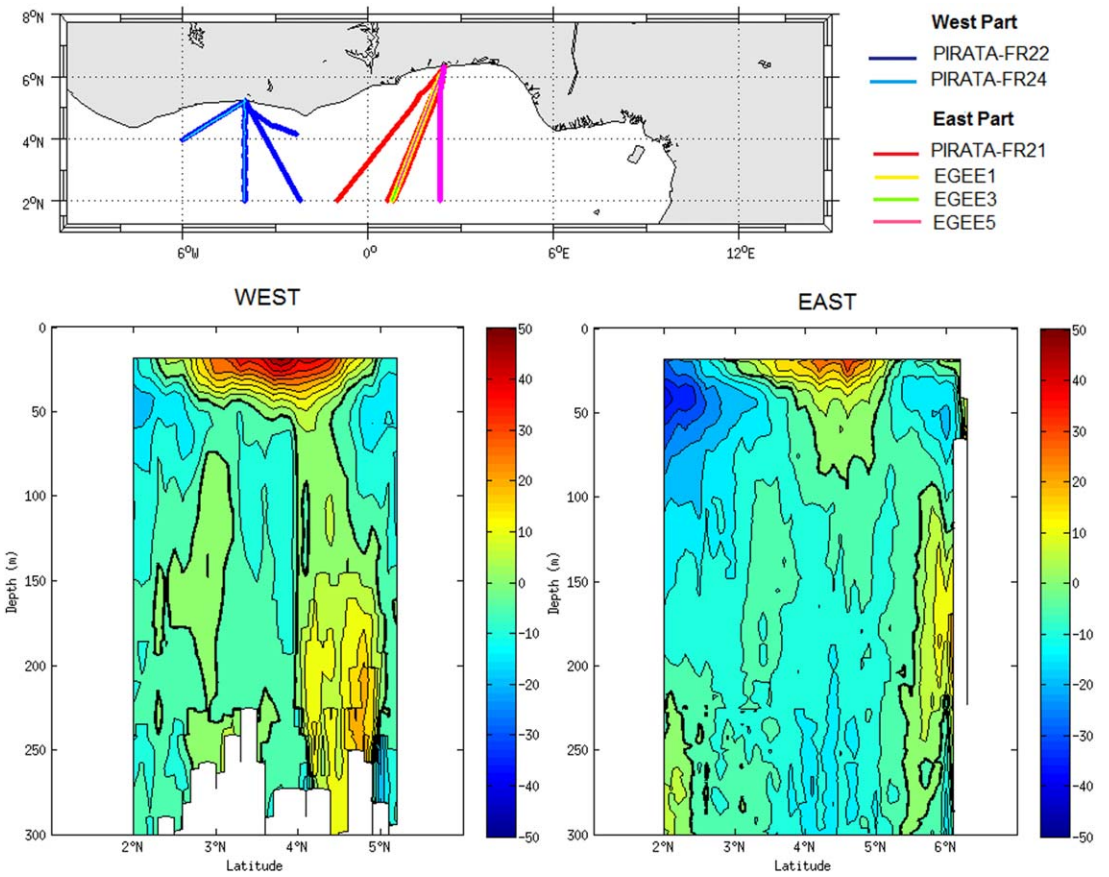

Figure 6. Averaged of zonal velocities (cm.s^{-1}) over April–May–June from (left) six sections located West of Cape Three Points and (right) eight sections located East of Cape Three Points. The map above indicates the used sections for compute the mean (in blue and cyan in the western part and in pink, red, yellow and green in the eastern part). Note that for the western part, data are available down to 150/200 m only for two sections.

100 m for 22/33 sections) than in fall (from September to November) (50 m for 5/8 sections). Its lower part is more difficult to estimate given the depth range of the SADCP measurements (~200 to 300 m).

In addition, to estimate the robust component of the eastward subsurface signal attributed to the GUC, the mean of the vertical distribution of zonal velocities from 2°N to the north coast of Gulf of Guinea has been calculated for April–May–June period by combining SADCP sections in two distinct areas: 6 sections West of Cape Three Points around 4°W and 8 sections East of Cape Three Points around 2°20′E. These averaged sections are shown on Figure 6.

In spite of large variability (more important around 4°W), the results clearly confirm that the GUC is a robust component of the circulation in this region and that it exhibits different patterns along both longitudes, as already summarized from individual sections. Around 4°W, the GUC is located from 150 m to 250/300 m depth and north of 4°N, whereas around 2°20′E, it is located from 100 m to 200/250 m depth and north of 5°N, trapped to the coast.

3.2. Salinity Properties of the GUC

In order to explore the potential origin of the GUC, we analyzed the salinity concentration, when in situ data were available, as this parameter can be used as a tracer to follow salt enriched waters coming from the west into the Gulf of Guinea through the EUC [e.g., *Gouriou and Reverdin*, 1992; *Mercier et al*., 2003; *Kolodziejczyk et al*., 2009] and their recirculations north and south of the equator [e.g., *Lemasson and Rebert*, 1973a,1973b; *Kolodziejczyk et al*., 2014]. We chose to show the salinity distribution along the 2°50′E sections in June 2005 and September 2005 and along 2°20′E in November 2006, (Figure 7) i.e., at different year periods and measured, along with the zonal currents described above during the same cruises (Figures 3 and 4).

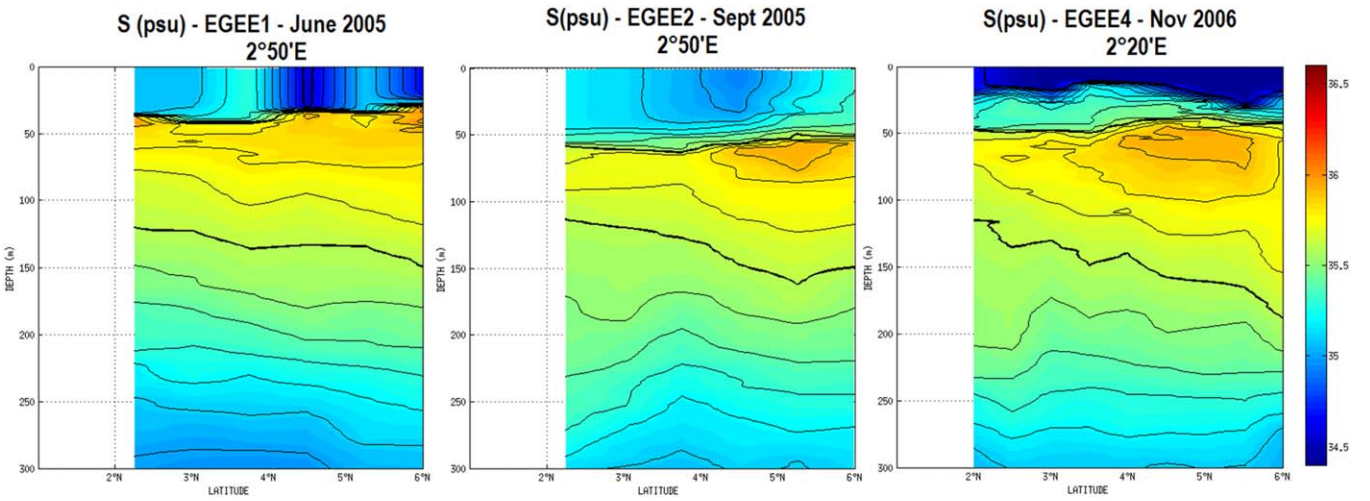

Figure 7. Vertical sections of salinity (psu) down to 300 m depth from CTD measurements obtained during the EGEE1, EGEE2 and EGEE4 cruises, respectively along 2°50′E in June 2005, 2°50′E in September 2005 and 2°20′E in November 2006.

We observe a layer of relative salinity maxima that extends over the whole sections from 2°N to the African coast in the 50–100 m depth range, with a salinity core (up to 35.9 psu) around or just below 50 m depth. In the literature, this salinity maximum is explained by eastward advection in the area of subtropical waters. During the EGEE4 cruise, the eastward flow highlighted in 50–250 m depth layer in Figure 3 is associated with a salinity maximum. Also, during the EGEE1 cruise, although less obvious, a slight salinity maximum is noticed close to the coast at the location of the eastward flow in the 50–150 m depth layer. During the EGEE2 cruise, the association between the eastward subsurface flow and the salinity maximum is less obvious.

Such observations induce some questions: 1) is the subsurface eastward flow observed around 100–250 m depth close to the coast the result of a direct advection from the west or of local recirculation? 2) what is the seasonal variability of this flow, that apparently may reverse to a westward flow? 3) is the GUC, defined as the subsurface eastward flow observed below the GC with a relative velocity maxima in the 100–250 m depth range, linked to the GC, part of it, or signature of local circulation pattern?

4. Presentation of Numerical Results

Despite of the large quantities of current measurements obtained during the cruises carried out in the Gulf of Guinea since 1995, the spatial and temporal distribution of the measurements is not sufficient enough to investigate the spatial and temporal variations of the circulation in the area. For this reason, we use the results of a numerical simulation to better understand the characteristics and variability of the circulation north of the Gulf of Guinea.

4.1. Model/Data Comparisons

Comparisons with in situ observations have been performed. Temperature and salinity data and SADCP measurements available every 2 min and from 16 m to 250 m depth have been compared with their values obtained at the grid points of the climatological model which correspond to the cruise track and the period of measurement. Since the in situ measurements are averaged every 2 min along the section, there is a 1 day period between the measurements obtained at 2°N and the ones obtained at the coast, while the numerical results are monthly averaged. The comparisons have been made for all vertical sections of zonal velocities available from cruise measurements. The Figure 8 shows examples of results obtained for three of them: at 2°20′E and from 2°N to 6°N on June (compared with SADCP measurements obtained during EGEE5 cruise in June 2007); at 7°W from 2°N to the coast and at 4°W from 2°N to the coast on April (compared with SADCP measurements obtained during PIRATA-FR22 cruise in April 2012).

For all the sections, the comparisons indicate that the model is able to reproduce the general characteristics of the observed circulation. The GC is present between 2°30′N and the coast with a vertical extension of

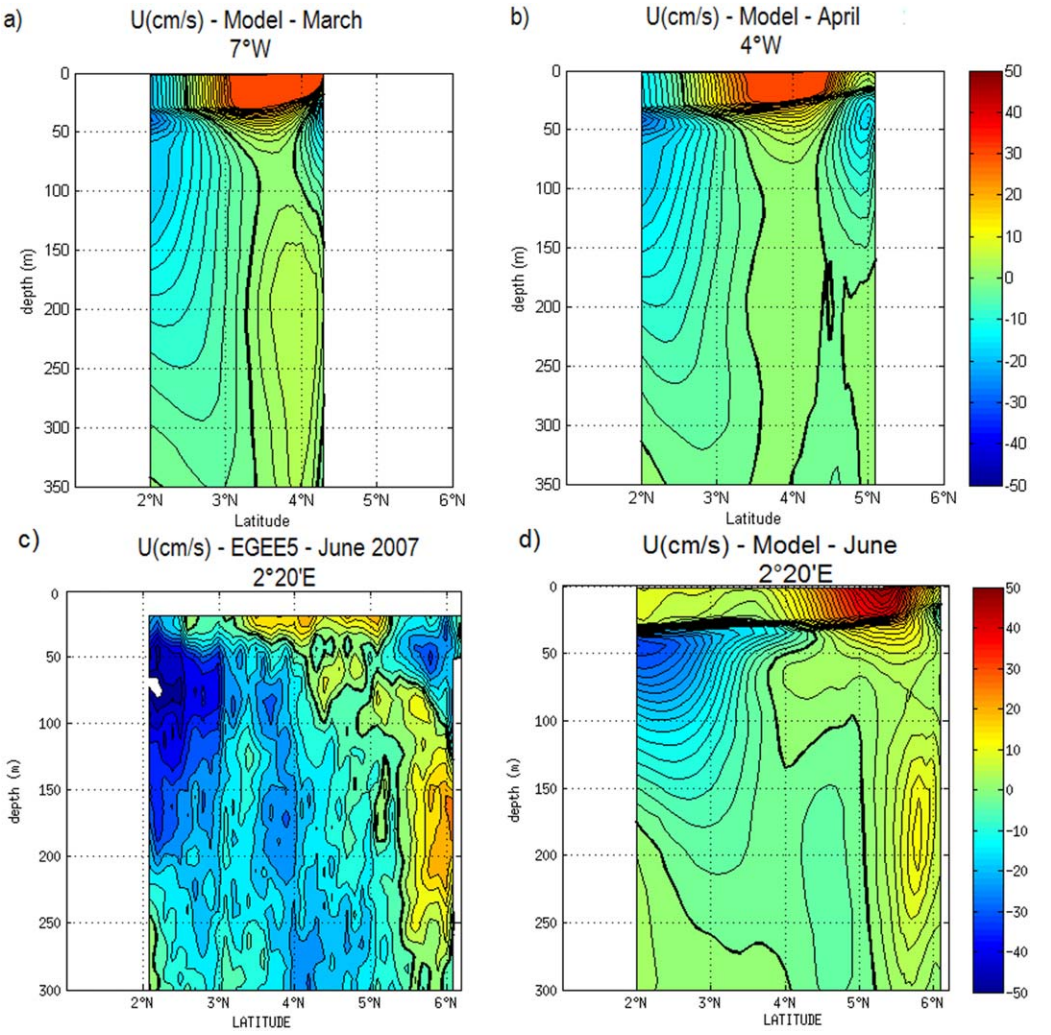

Figure 8. Vertical sections of zonal velocity (cm.s^{-1}) down to 300 meters depth from the model at (a) 7°W and (b) 4°W in April (compared with the equivalent from SADCP measurements presented in Figure 4). (c) Same but at 2°20′E from SADCP measurements obtained during the EGEE 5 cruise in June 2007, and (d) the equivalent simulated by the model. The instantaneous current measurements are compared with monthly averaged outputs of the climatologic numerical child model.

about 40 m depth and zonal velocities reaching 50 cm.s^{-1}, surrounded by the two westward flows: the GCC, in a opposite direction of the GC and close to the coast, is well-established (values around 10 cm.s^{-1}) compared to observations at 7°W and thicker than observation at 4°W; and the nSEC south of the GC and extending at least down to 250 m depth. The eastward GUC is also simulated by the model, even with slightly weaker velocities than observations (around 10 cm.s^{-1} against around 20 cm.s^{-1}), and at slightly different depths or latitudes than observations, that may be partly explained by the thicker simulated GCC located just above. At 4°W, we can also notice a thin eastward vein trapped to the coast from 50 m to at least 250 m depth, in agreement with observations (Figure 5 and Table 1). The simulated zonal velocities at 4°W and 2°20′E are also consistent with the mean sections calculated for April–May–June from SADCP data around 4°W and around 2°20′E previously shown on Figure 6, indicating that the model reproduces these robust components of the GUC in this area during spring.

Similar comparisons have been made with salinity and temperature sections drawn from available CTD measurements and numerical results.

Figure 9 shows three vertical sections of salinity at 7°W, 4°W and 2°20′E obtained respectively during two legs of the PIRATA-FR22 cruise in April 2012 and during the EGEE5 cruise in June 2007. The figure can be analyzed in tandem with zonal currents presented along the same sections in Figures 5 and 8. For each

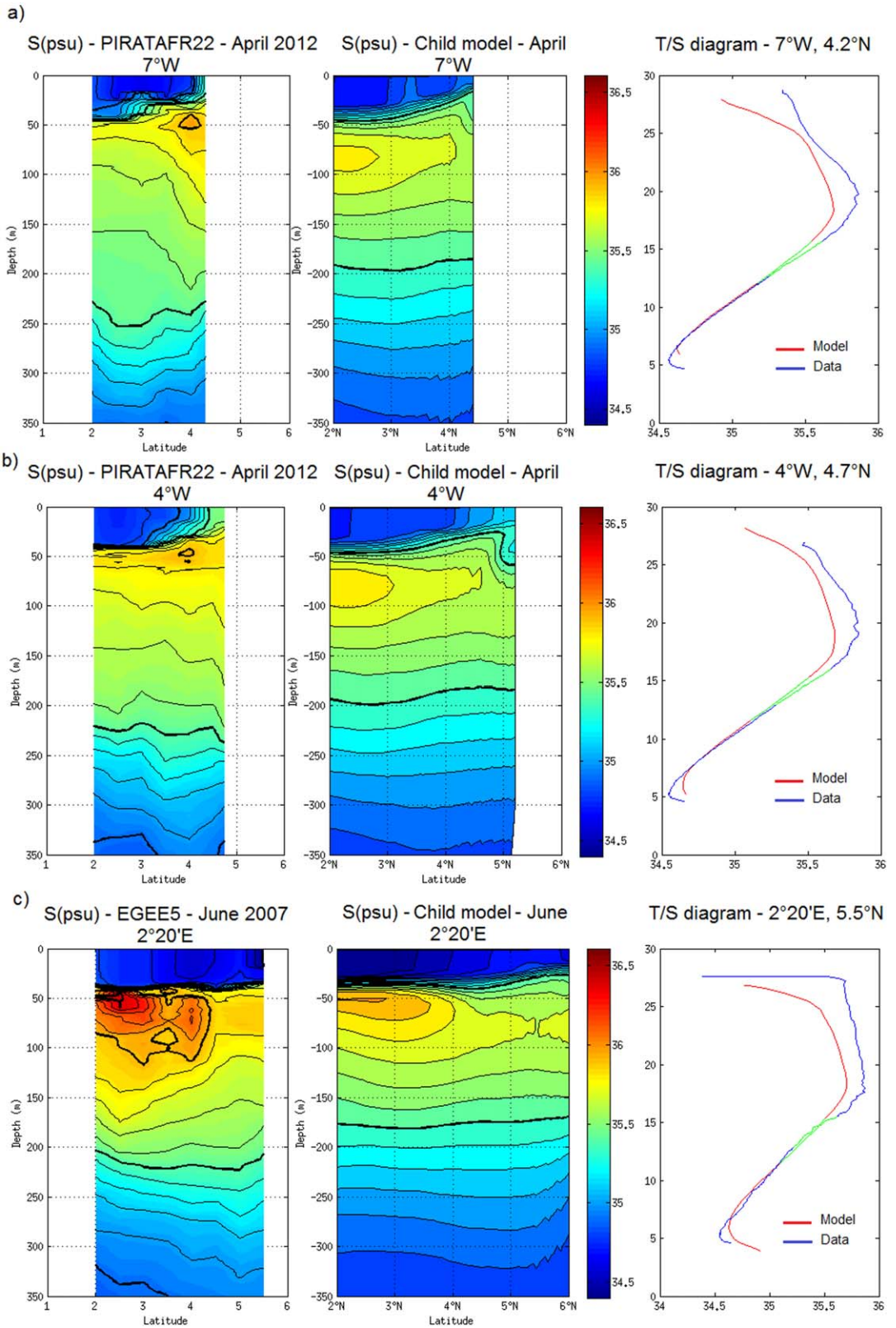

Figure 9. Vertical sections of salinity (psu) down to 350 m depth and from 2°N to 6°N, from CTD measurements obtained during the PIRATA-FR22 cruise and simulated by the child climatological model (monthly averaged) along the section (a) 7°W and (b) 4°W on April 2012; and during the EGEE5 cruise along (c) 2°20'°E on June 2007. For each section, a T/S diagram for a point located in the GUC (based on zonal velocity section presented in figure 8) is shown for the model and for CTD measurements. The green curves indicate the temperature and salinity from 150 m to 250 m depth, where the GUC is present.

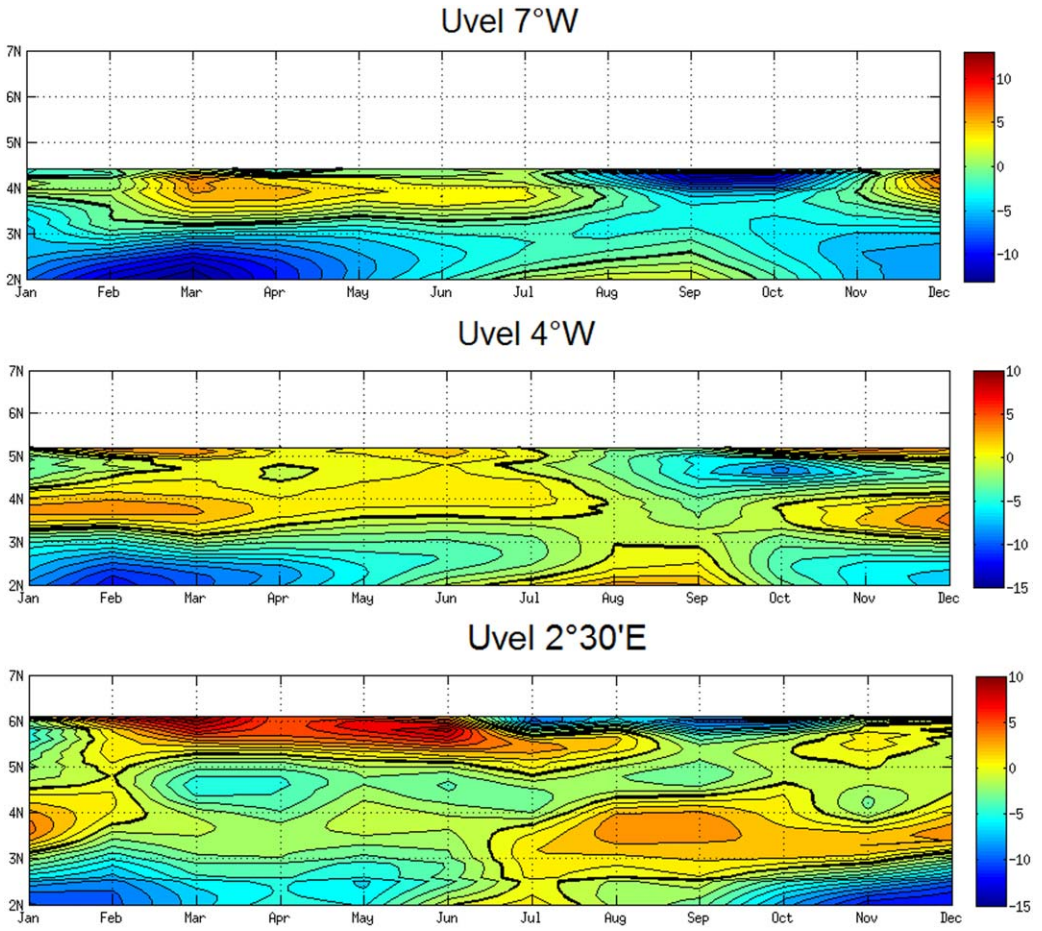

Figure 10. Hovmoller diagrams of monthly averages zonal velocity (cm.s^{-1}) simulated by the child model and averaged between 150 m and 250 m depth at (top) 7°W, (middle) 4°W, and (bottom) 2°20′E from 2°N to 7°N over the climatologic year.

section a T/S diagram at the latitude where the GUC is observed and simulated is also shown. The green curves indicate the temperature and salinity from 150 m to 250 m depth, where the GUC is present. Along the 3 sections, the simulated salinity is generally fresher than observations, up to 0.1 psu in the upper GUC and about 0.2 psu in the upper layers. These differences can be partly explained by a bias in the mean circulation pattern in the upper layers and by the fact that we compare instantaneous salinity measurements with monthly averaged outputs of the climatologic numerical model, at one specific point. Thus, the high frequency variability presents in in situ measurements are largely filtered in the numerical outputs. However, for the three longitudes, the T/S diagrams show that the salinity variations and maxima are relatively well reproduced, allowing to follow significant water masses associated to the main currents.

The reliability of the model for its vertical structure (temperature, salinity and velocity), particularly in the equatorial band, has also been successfully tested by comparison with the annual mean of velocity, temperature and salinity, obtained by *Kolodziejczyk et al.* [2009] from 18 sections carried out along 10°W (not shown).

4.2. Seasonal Variability of the GUC

Figure 10 shows the zonal velocities averaged from 150 m to 250 m depth at 7°W, 4°W and 2°20′E and from 2°N to the coast over the climatologic year.

At 7°W, the eastward current in the 150–250 m depth layer is well present from November–December to July–August along the 4°N latitude, and replaced by a westward current from September to November. The highest eastward velocities (around 5–10 cm.s^{-1}) are observed in March–April and December. At 4°W, two eastward currents are clearly visible: one along 4°N, as at 7°W, and the second one trapped to the coast.

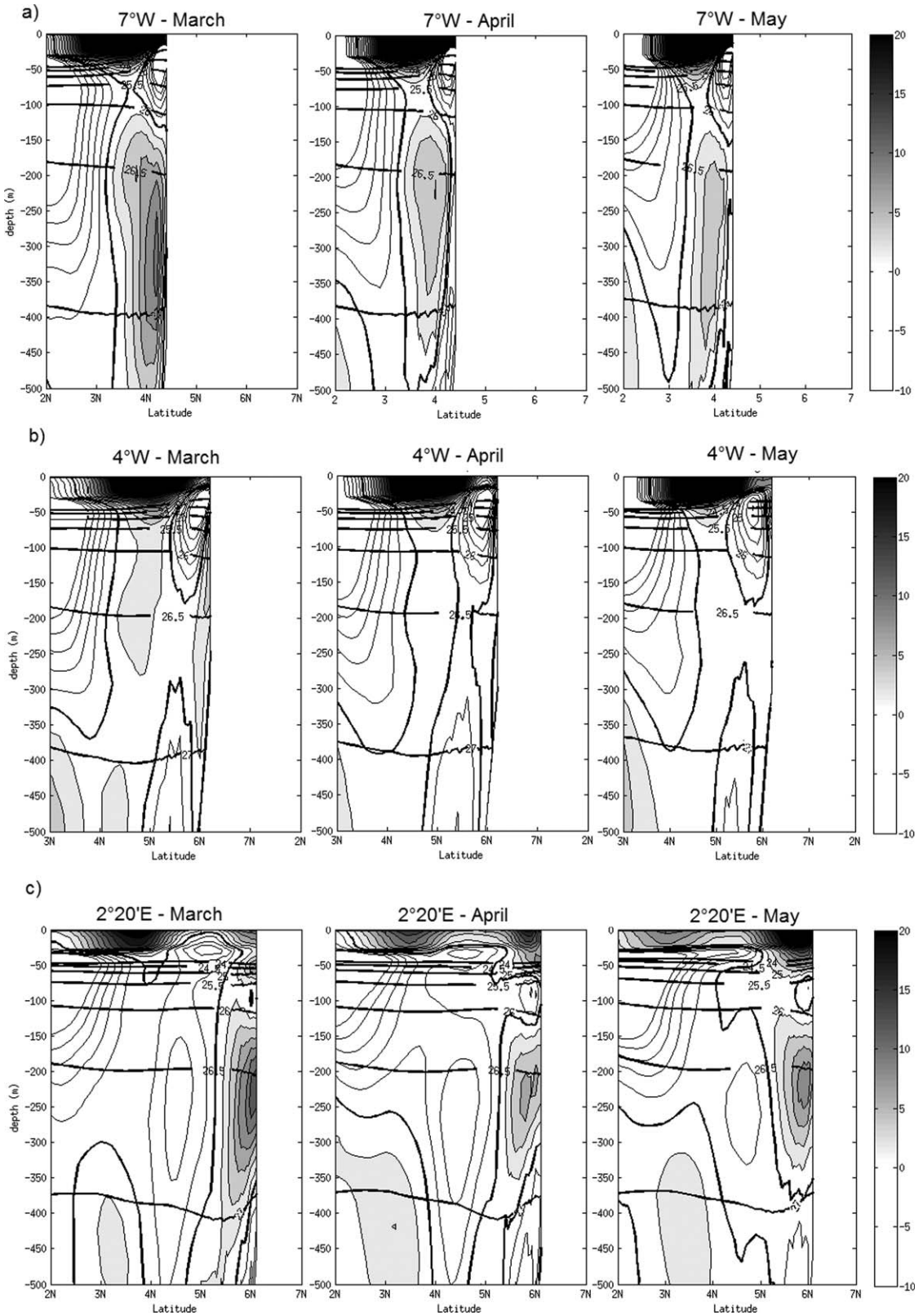

Figure 11. Depth-latitude sections of monthly average of zonal velocity (cm.s^{-1}) simulated by the child model from the surface to 500 m depth over March, April, and May at (a) 7°W, (b) 4°W, and (c) 2°20′E and between 2°N to 7°N.

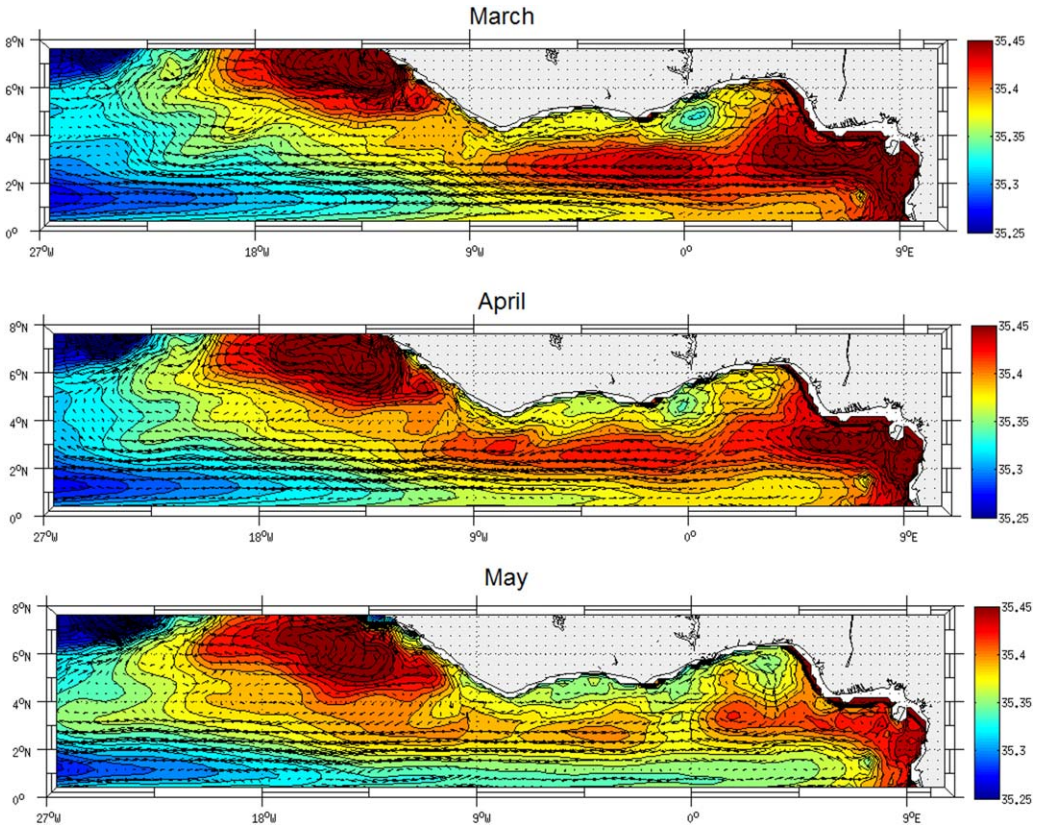

Figure 12. Maps of monthly salinity (psu) averaged between 150 and 250 m depth for March, April, and May, superimposed with horizontal velocity vectors, as seen by the climatological model. Speed is proportional to the length of the tail of a vector. Every 2 vectors in meridional and zonal directions are shown.

Both currents are present most of the year and replaced by westward flows from August to October. At 2°20′E, two eastward currents are also present; around 3–4°N it is mostly visible from July to January, while at the coast it appears from February to August and from October to December, with highest amplitude in March and May–June. In July–August and October–November, it is further off the coast that from February to June. One might raise the question whether the eastward current observed around 3–4°N at 2°20′E from October to December is an eastward continuation of the one simulated at 7°W and 4°W or has another origin. Furthermore, as previously noticed from comparisons between observation and model results (Figure 8), the eastward velocities are slightly weaker at 4°W than at 7°W and 2°20′E (maximum velocity core around 7 $cm.s^{-1}$ at 4°W) maybe suggesting a recirculation zone offshore of Cape Palmas and in the eastern part of Gulf of Guinea which would reinforce the eastward flow at this location.

In order to verify the vertical distribution of eastward velocities over the year and to give more details about the eastward flow trapped to the coast, the depth-latitude sections of monthly averaged zonal velocities at 7°W, 4°W and 2°20′E are shown in Figure 11 for March, April and May months. The eastward flow extends from 100/150 m to 350/450 m depth with a maximum velocity core around 250/300 m depending of locations. A strengthening of the flow at three locations in March is clearly depicted, in agreement with previous results. In addition, the current is located between roughly the same isopycnal surfaces (26 and 27 $kg.m^{-3}$) for the three different locations indicating a connection between the currents at the west and at the east of the Gulf of Guinea. At 4°W, a thin eastward component trapped to the coast is observed around 200 m depth over the 3 months, in agreement with observations (Table 1) and previous results (Figure 10). In addition to the GUC, we also noticed the westward 50/100 m depth flow under the GC identified as the GCC by *Lemasson and Rebert* [1973b]. For the locations shown here, we do not notice any particular linkage between the GUC and the GCC.

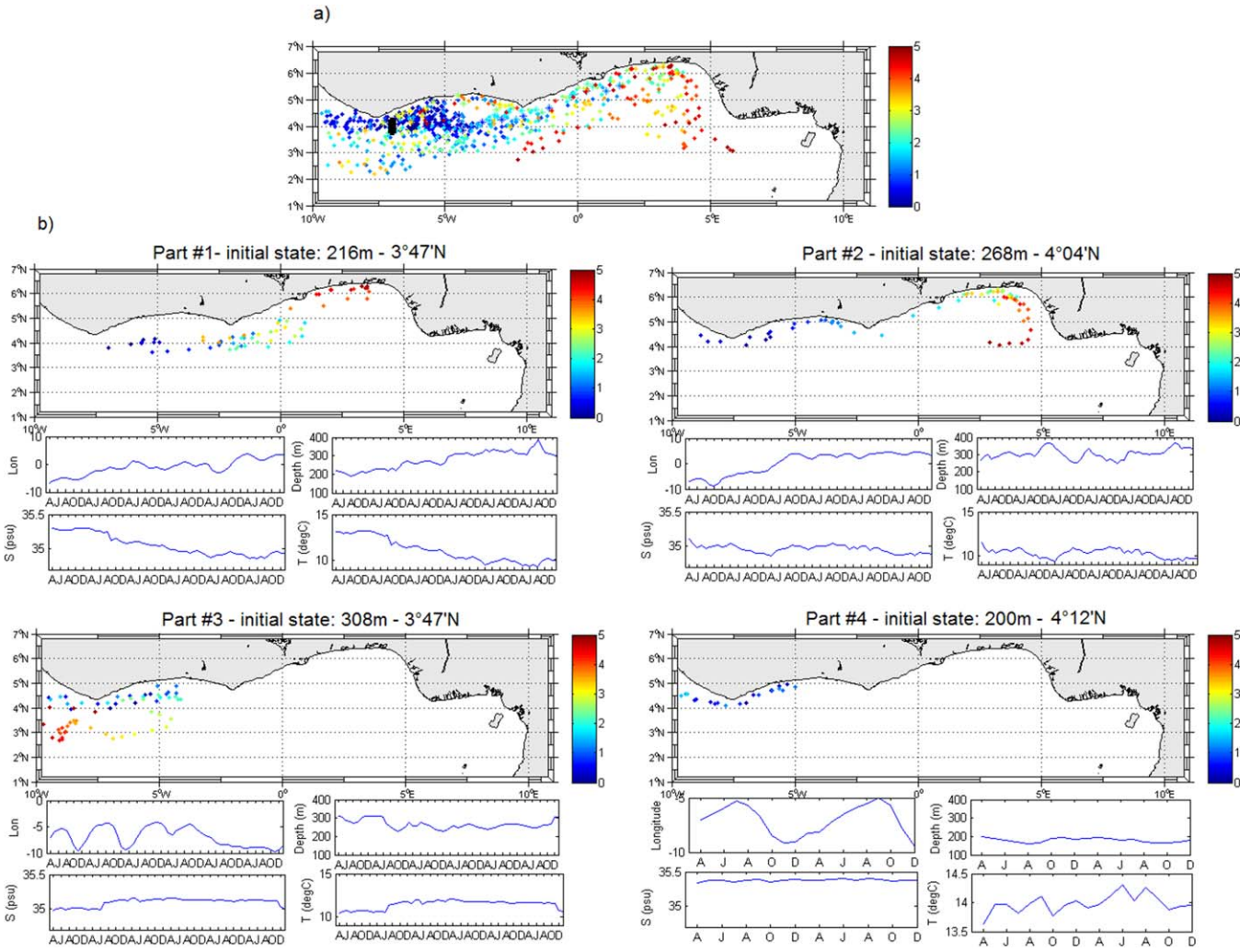

Figure 13. Pathways of the GUC water masses from 7°W followed forward in time cycling over 5 years from April to March. The particles are released in GUC waters on April, uniformly distributed on the vertical between 150 m and 250 m depth. Positions are indicated every month with color-coded dots, where the color indicates the time since the release of the particles (5 climatologic years). (a) All the obtained pathways. The starting points of particles are marked by black stars; (b) four typical trajectories representative of the major pathways and along-trajectory variations of longitude, depth (in meters), temperature (in °C) and salinity (in psu), function of months (X axis labels are "AJAOD" for "April June August October December").

In order to have a global examination of current and salinity pattern in the 150–250 m layer in the study region and their seasonal variability, we show in Figure 12 maps of monthly salinity averaged between 150 m to 250 m depth superimposed with vector velocity, as simulated by the climatological model.

The modeled velocity distribution and salinity field in 150–250 m depth layer over the climatologic year show well-known patterns of this region. We notice a westward recirculation of salinity maximum waters along ∼3°N which corresponds to the lower part of nSEC flow (around 35.4–35.5 psu), fed by a northern EUC recirculation in the far east of the Gulf of Guinea [*Kolodziejczyk et al.*, 2014]. Another maximum salinity zone is also present in the northwestern region, associated with an anticyclonic circulation related to a downward displacement of isotherms. The two high-salinity tongues join in spring (Figure 12, March map) accompanied by a southward inflow in the eastern basin along the continental slope of West African coast and the northern coast of Gulf of Guinea. This eastward subsurface flow along the coast is in agreement with previous results, i.e., highest transport in boreal spring and a weakening during fall and winter (not shown). In summer (not shown) this current effectively reverses westward, associated with fresher water ($<$ 35.35 psu), and reinforces the northward flow along the Northwest Africa coast. Otherwise, the March map depicts an anticyclonic circulation off Cape Palmas suggesting strong recirculation in this region that can explain, at least partially, the stronger eastward velocities noticed at 7°W.

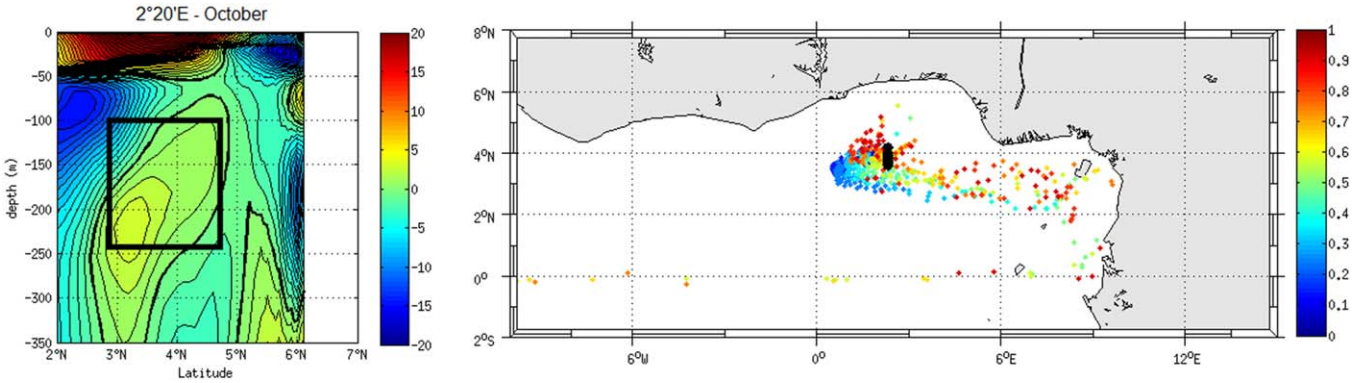

Figure 14. Depth-latitude section of zonal velocity (cm.s^{-1}) at 2°20′E in October. The black square indicates where the particles are released: from 3°N to 4°N in 100–250 m depth layer (left plot); Trajectories distribution map for the investigation of the origin of this eastward flow. 50 particles were deployed and followed backward in time using the monthly averaged velocity fields of the climatological child run for 1 year. Positions are indicated every month with color-coded dots, where the color field indicates the time running backward from the release of the particles (1 climatologic year).

4.3. GUC Pathway and Sources

The analysis of in situ measurements obtained from the cruises carried out north of Gulf of Guinea since 1983 highlighted the presence of an eastward current, the GUC, located from 50/150 m to 200/300 m with mean velocities of 10 cm.s^{-1}. The comparison with our climatological simulation results showed that this current is also present in our numerical simulation even though most often associated with slightly weaker velocities than from observations. This raises the question whether there is continuity between the eastward GUC observed and simulated from Cape Palmas to Cape Three Points and the eastward current observed and simulated in the East of Cape Three Points, or whether this last one is attributable to a local recirculation. To this end, Lagrangian trajectories have been computed from numerical outputs using the ARIANE Lagrangian diagnostic tool.

4.3.1. Pathway of the GUC Along the Northern Coast of Gulf of Guinea During Spring

In order to map the main Lagrangian pathways of the GUC and to assess the connection between the eastward subsurface flows observed and simulated north of 3°30′N west and east of Cape Three Points, ARIANE was used in qualitative mode: 27 particles are launched between 150 m to 250 m depth, uniformly distributed in the patch of water flowing eastward between 3°47′N and the coast on April at 7°W (Figure 13). The initial positions of numerical particles have been chosen according to the analysis of SADCP measurements and from numerical results, which attested the presence of an eastward subsurface current in this patch of water (see section III-1 and IV-1 and especially Figure 8). We chose to compute the trajectories cycling over 5 years from April to March. Figure 13a shows all Lagrangian pathways.

The starting points of particles are marked by black stars. The trajectories highlight strong recirculation regions as well as the major pathway of the particles. They also clearly display a connection between waters located west and east of Cape Three Points. In particular, four main pathways scenarios are identified and presented in Figure 13b through the trajectories of four particles associated with the along-trajectory variations of their longitude, depth, temperature and salinity. The first particle illustrates the pathway of the GUC from West to East of the Gulf of Guinea. It travels eastward along the latitude 4°N from Cape Palmas to Cape Three Points and follows the coast until 3°30′E after around 4 years while gradually deepening from 216 m to 400 m. Its eastward displacement is not direct from west to east but interrupted by current reversal during August–December period especially off Cape Palmas and off Cape Three Points. The second particle, initially placed closer to the coast, at 4°04′N, and at 268 m has a similar pathway except that it follows an eastward flow trapped to the coast before reaching (more directly) the eastern part of the Gulf where it veers back (within the westward flow identified as the nSEC). The presence of this eastward coastal flow between the Cape Palmas and the Cape Three Points is consistent with the one identified on Figure 10 and 11 and suggested from SADCP measurements (Figures 5 and 8b; Table 1).

The two other particles indicate strong recirculation off Cape Palmas. The third particle, initially placed at 308 m and 3°47′N, suggests that a portion of the GUC is fed by anticyclonic recirculation off Cape Palmas, including lower part of the nSEC waters. Finally the trajectory of the fourth particle, initially placed closer to the coast, evidences the strong variability of currents flowing alternately eastward (from December to July)

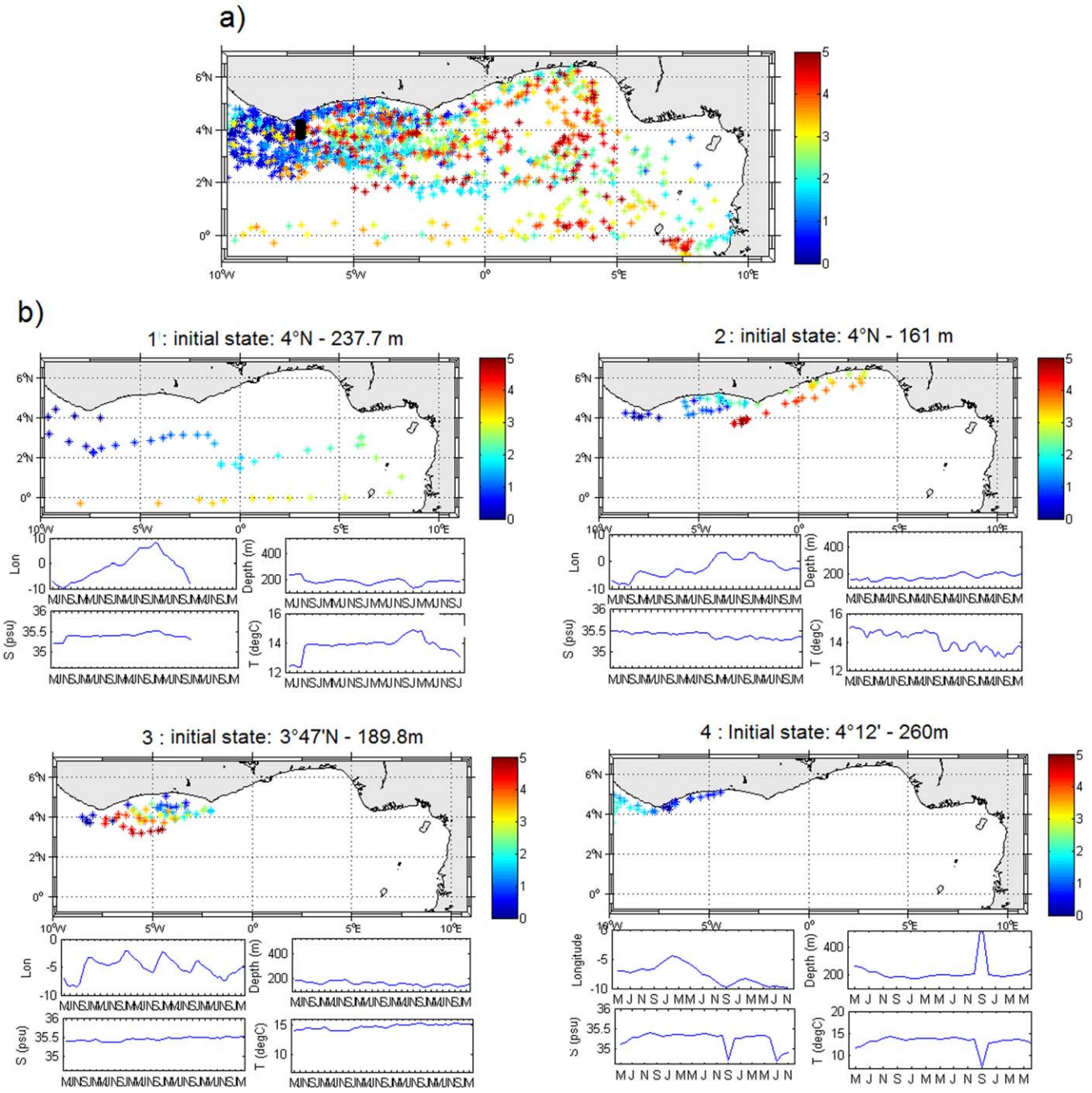

Figure 15. Trajectories distribution map for the investigation of GUC sources. The particles were launched at 7°W in GUC waters depths, i.e., from 150 m to 250 m depth on April, and followed backward in time using the monthly averaged velocity fields of the climatological run for 5 years. Positions are indicated every month with color-coded dots, where the color field indicates the time running backward from the release of the particles (5 climatologic years). All trajectories are shown in Figure 15a while the four typical trajectories illustrating the major source pathways and along-trajectory variations of longitude, depth (in meters), temperature (in °C) and salinity (in psu), function of months are shown in Figure 15b)(X axis labels are "AJAOD" for "April June August October December"). The starting points of particles are marked by black stars.

and westward (from August to November) along the African coast, as observed on Figure 10 (suggesting a link with more western waters). The temperature and salinity associated with GUC waters are ranged respectively between 10 and 14°C and between 35 and 35.4 psu.

These results are in agreement with the analysis of SADCP measurements and provide a better understanding of the GUC dynamic. They also attest a direct connection between the 150–250 m depth eastward

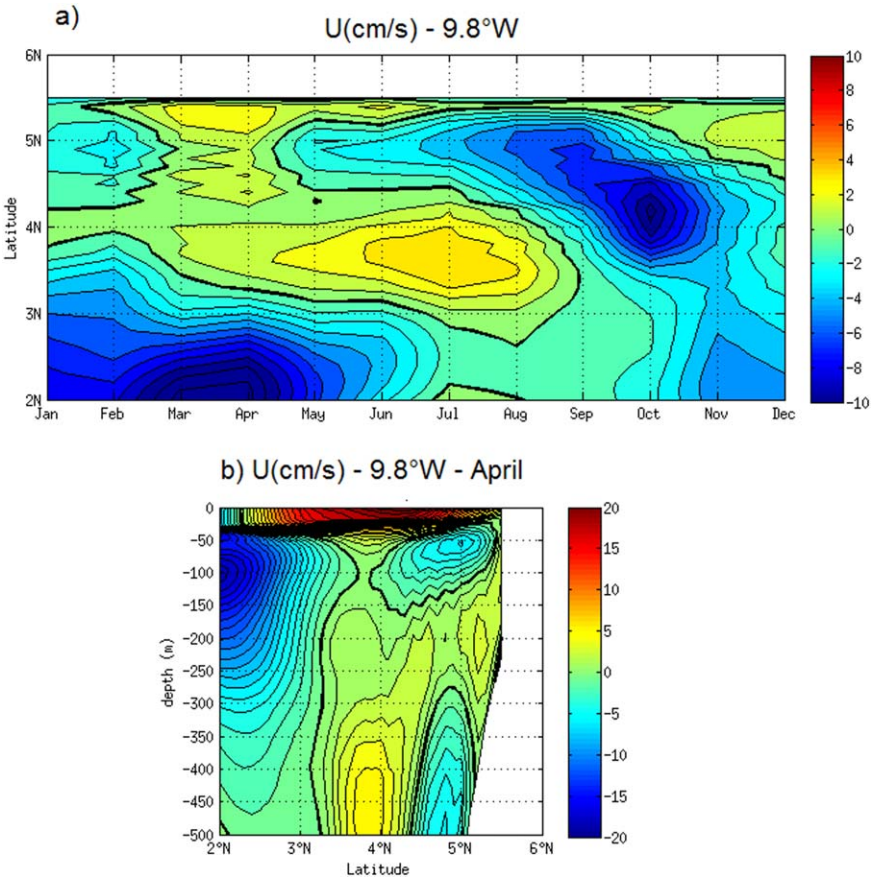

Figure 16. (a) Hovmoller diagram of the zonal velocity (cm.s^{-1}) over climatologic year averaged from 150 m to 250 m depth along 9°48′W, and from 2°N to the coast. (b) Depth-latitude section of monthly average of zonal velocities (cm.s^{-1}) over April from the surface to 500 m depth simulated by the child model at 9°48′W and from 2°N to 6°N.

currents observed in the west, off Cape Palmas, and in the east, off Cape Three Points. In particular, the results suggest that the GUC flows along the coast east of Cape Three Points. That raises the question about the origin of the eastward flow simulated in 150–250 m depth layer around 3–4°N at 2°20′E during October–December months (Figure 10). To address this question, a backward-in-time experiment has also been performed. The goal is to get information about the source regions of water parcels found within a predefined release zone. In the present case, 50 particles are deployed in the eastward flow located in the 100–250 m depth layer at 2°20′E between 3°N and 4°N on 1 October and followed them backward in time with maximum transit time of 1 year.

The so-obtained trajectories (Figure 14) clearly indicate that the eastward current observed around 4°N at 2°20′E is not an eastward continuation of the GUC observed at 7°W and 4°W, but a regional recirculation of EUC waters limited to the eastern part of the Gulf of Guinea. Similar results have obtained whit a release date in January and August (not shown).

4.3.2. Origin of GUC Waters at 7°W

In order to investigate the GUC sources at 7°W, we performed another backward-in-time simulation. We released simultaneously 27 particles from 150 m to 250 m depth within the GUC at 7°W (see Figure 8) on April and followed them backward in time with maximum transit time of 5 years. The results of the experiment as well as four typical trajectories are presented in Figure 15.

Figure 15a reveals a highest concentration of particles in the area of the release zone suggesting this region to be the place of strong recirculation. We can distinguish four main groups of pathways illustrated respectively by the pathways of the 4 particles shown in Figure 15b. The first group (particle 1; top-left plot) indicates that the GUC is partly fed by EUC waters, as revealed by the trajectory of this particle which recirculates from the EUC through the nSEC and reaches the GUC at 7°W with a transit time of around 3

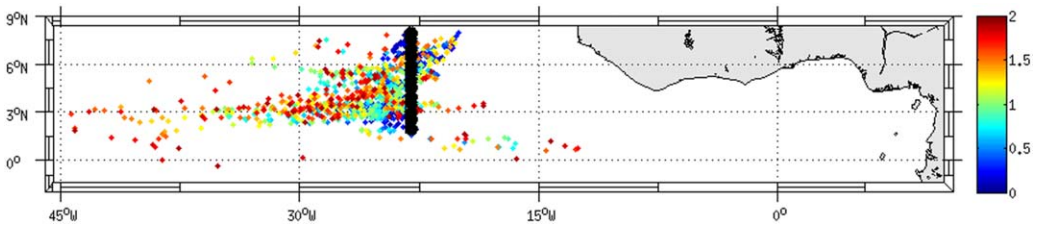

Figure 17. Lagrangian trajectories obtained from qualitative forward experiment using monthly velocity fields from parent model. The black circles indicate the section along which the particles are initially released: at 23°W from 2°N to 8°N (black circles) and from 150 m to 250 m depth on January. The color field is the time since the release of the particles (2 climatological years).

years. The mixing between the salty and warm EUC waters with lower nSEC waters is clearly identified by a change in physical properties of the particle during the second year September month: the temperature and salinity along-path effectively drop by 0.1 psu and 1°C respectively. Otherwise, the group 2 (particle 2; top-right plot) reveals a recirculation cell along the coast, characterized by a horizontal zigzag path from west to east due to the eastward to westward reversal of the subsurface current during August–September months (Figure 10). As a result, the travel time of the particles that transit from 7°W to the eastern part of the Gulf of Guinea is generally longer than 3 years. Another anticyclonic recirculation pattern is observed off Cape Palmas and concerns the particles of the third group (particle 3; bottom-left plot), initially released at depths superior or equal to 200m. Finally, the fourth group (particle 4; bottom-right plot) pathways show that particles also originate from the west (northwest, north of 4°N), out of the domain. Thus, the Lagrangian experiment reveals that the GUC is fed through three main source pathways: (1) strong recirculations due to the seasonal variability of the current; (2) recirculation of EUC and lower nSEC waters; and (3) inflow coming from outside of the domain northwest of 4°N-7°W.

To better investigate the source of the inflow coming from west, we checked the zonal velocity yearly variations at the western boundary of the child model (9°48′W), averaged between 150 and 250 m depth, shown in Figure 16 (bottom). This figure can be analyzed in tandem with the Hovmoller diagrams at 7°W, 4°W, and 2°20′E presented in Figure 10. It shows that the seasonal variability of the eastward flow entering the Gulf of Guinea at 9°48′W north of 3°30′N is well correlated with the GUC's one: it also exhibits a velocity maximum in April, and the flow becomes westward in September–November. Furthermore, as previously noticed at 7°W and 4°W, we can identify two eastward flows: one coastally trapped around 5°N, and another one around 4°N. These two flows are clearly visible on depth-latitude section of zonal velocities average over April month shown on Figure 16 (bottom).

We also wonder whether the eastward flow entering in Gulf of Guinea north of 4°N is the extension of a more northern coastal current or whether it is a continuation of the NEUC. Presently, the NEUC flows eastward at similar water depths than the GUC and has been observed at 23°W around 5°30′N [e.g., *Bourlès et al*., 2002]. Nevertheless, the water mass characteristics of the GUC north of 3°30′N (relatively low salinity and temperature; Figure 9) do not correspond to those of the NEUC. To address these questions, we have conducted additional backward Lagrangian experiments using the monthly velocity fields of the parent climatological simulation, which has, although a larger spatial resolution than the child model, a domain extending up to 8°N and 60°W. 69 particles were released at 23°W, between 2°N and 8°N and from 150 m to 250 m depth, i.e., around the NEUC latitudes and depth ranges. To consider the seasonal variability, the trajectories were started from different release times (January, April, August, and November) and integrated forward in time with a maximum cycling time of 2 years. Given that the main pathways obtained are very similar regardless of the release date, we only show the trajectories obtained for particles released on January (Figure 17).

No particle released at 23°W north of 4°N in 150–250 m depth layer enters the Gulf of Guinea over 2 climatological year and all of them effectively shift northward within the Guinea Dome, regardless of the time of year. This result is in full agreement with several authors [e.g., *Hisard et al*., 1976; *Arhan et al*., 1998; *Stramma and Schott*, 1999; *Bourlès et al*., 2002] who already suggested that the NEUC does not penetrate into the Gulf of Guinea. Thus, the coastal inflow at the northwestern boundary of the Gulf of Guinea in 100–250 m depths layer can only be an extension of a coastal current coming from more northern latitudes.

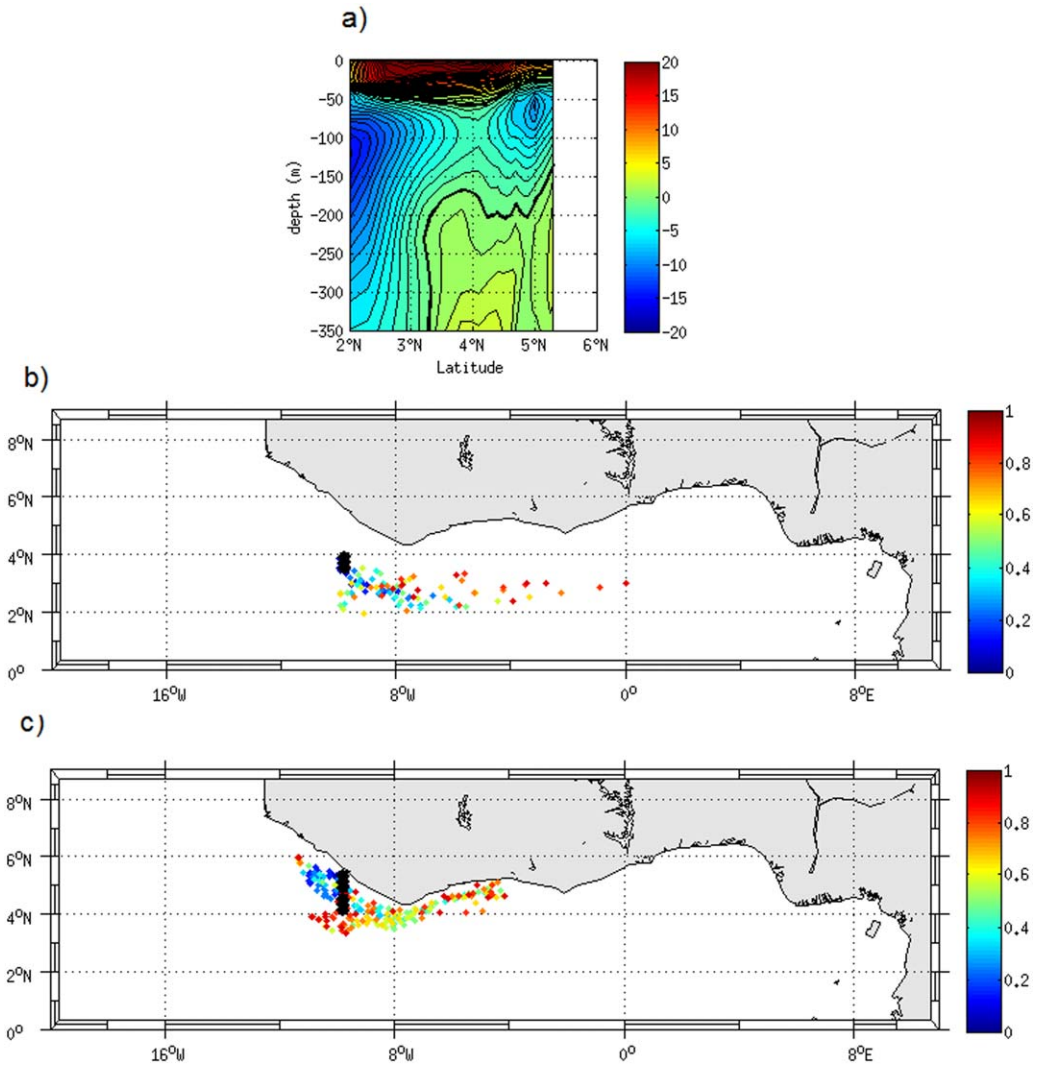

Figure 18. (a) Hovmuller diagram along 9°48′W of zonal velocity field averaged over April, between 2°N and 6°N. (b, c, and d) Lagrangian trajectories obtained from qualitative backward experiment using monthly velocity fields from the parent model. The black circles indicate where the particles are initially released at 9°48′W on April: (b) from ∼180 m to 250 m depth, between 3°30′N to 4°N (9 particles) and (c) from ∼130 m to 250 m between 4°N and 5°17′N (23 particles). The color field is the time running backward from the release of the particles (1 climatologic year).

To further examine the source pathways of the inflow which enters in the Gulf of Guinea at 9°48′W north of 3°N in the 150–250 m depth layer, a Lagrangian backward experiment was conducted using velocity field from the "parent" model. 9 particles have been released at 9°48′W in the eastward flow between 3°30′N and 4°N and between ∼180 and 250 m depth, and 23 other particles between 4°N and 5°17′N between ∼130 and 250 m depth on April and followed backward in time over 1 climatological year (Figure 18).

The results shown in Figure 18b indicate that all the particles, deployed within the eastward flow simulated on April at 9°48′W from 3°N to 4°N in the 180–250 m depth layer, originate from the east along 3°N through the retroflection of waters flowing westward along 2–3°N. *Stramma and Schott* [1999] described such retroflection of the nSEC in surface layer (0–100 m) during spring, fed itself by EUC waters which is deflected westward in the eastern part of Gulf of Guinea (their Figure 4). That suggests that at 9°48′W a lower part of nSEC waters veers eastward and provides the southern part of the GUC. The model trajectories suggest the sources of the particles released between 4°N and 5°17′N (Figure 18c) as recirculations of more coastal waters flowing along the northern coast of Gulf of Guinea as well as along the western coast, at higher latitudes. Indeed, the monthly salinity maps previously presented in Figure 12 also indicate a southward inflow which follows the West Africa coast and enters eastward in the Gulf of Guinea in March.

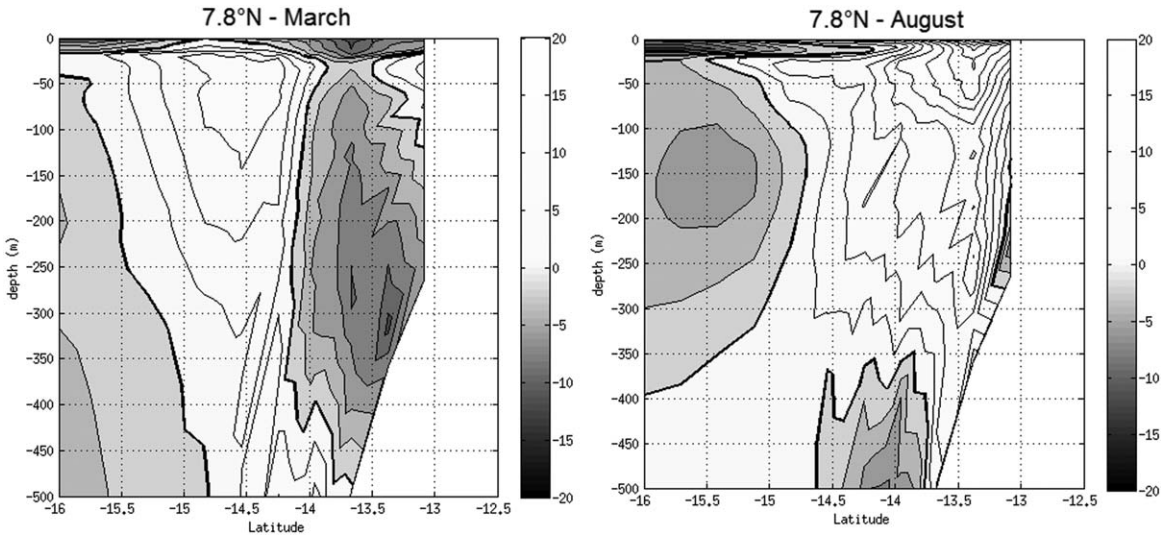

Figure 19. Depth-longitude sections of meridional velocity (cm.s^{-1}) averaged over March and August down to 500 m depth, at 7°47′N between 16°W and 12°30′W.

5. Discussion/Conclusion

The analysis of SADCP measurements obtained from several cruises carried out since 1995 in the Gulf of Guinea evidences the presence of an eastward flow in the 35.2–35.5 salinity layer north of 3.5°N from 100 m to 250 m depth with a mean velocity of 10 cm.s^{-1}. At some locations, the current is often associated with a salinity maximum, suggesting that it might be partly fed by EUC recirculating waters. Since the measurements obtained from the cruises are sparsely distributed along the year, a high resolution model, which reproduces the general circulation, helped us to better describe the complex circulation in this particular area. The model results showed that the eastward subsurface current reaches maximum velocities in March–April and reverses westward in August–September. The seasonal variability of the current is similar at the West and East of the study region, with higher eastward velocities at 7°W and 2°20′E due to local recirculations which reinforce the current at these locations, bringing relatively salty waters. Lagrangian tracking results confirmed the presence of strong anticyclonic recirculation patterns mainly in two particular areas: off Cape Palmas and east of Cape Three Points including recirculations of nSEC with relatively warm and salty waters. We also identified two distinct eastward flows at 150–250 m depth. The first one flows eastward below the GC around 4°N from Cape Palmas to Cape Three Points and follows the route close to the coast east of Cape Three Points. The second one is trapped against the coast between Cape Palmas to Cape Three Points. We have decided to call the eastward current below the GC the Guinea UnderCurrent (GUC), while the coastal eastward current is called the North Guinea Coastal UnderCurrent (NGCUC).

Lagrangian analysis also allowed us to corroborate that the GUC is not the extension of NEUC waters which would penetrate in the Gulf of Guinea, consistent with earlier observations [e.g., *Arhan et al*., 1998; *Bourlès et al*., 2002]. There have been speculations about such a connection. *Mercier et al*. [2003] suggested the possible presence of NEUC at 9°W around 2°30′N in January–March 1995 from observed subsurface currents (their Figure 7). From our model results, such eastward subsurface flow at this location is rather an eastward recirculation of lower nSEC waters. The investigation of the sources of the GUC and NGCUC at 9°48′W through Lagrangian backward-in time tracking shows that the southern part of the GUC is mainly fed by the retroflection of lower nSEC waters while the NGCUC receives a large part of its waters from a southward current flowing along the slope of West African coast. The along-slope circulation south of 10°N in the 100/250 m layer is still poorly documented. Nevertheless, from another high resolution model performed by *Elmoussaoui et al*. [2005], a similar southward current is present in upper Central Water ($26.2<\sigma<26.8$) during spring and fall and reverses northward in summer and winter (their Figure 13). The meridional velocity fields of our model in this area are in agreement with these results and depict a southward flow with similar seasonal variations. Figure 19 shows the meridional velocity averaged over March at 7°48′N along the West Africa coast. The southward flow is simulated from 50 m to 400 m depth from 14°W to 13°42′W. In August, this current is reversed northward.

Apart from the GUC, the analysis of SADCP measurements and model results reveal the presence of the GC in 0–50 m depth layer as well as the westward 50/100 m depth flow under the GC as described by *Lemasson and Rebert* [1973b], without any clear link with the GUC variability. Nevertheless, although the concerned water layer differs, the spring pattern of the GUC fate and its source pathways can recall the source of the GC described by *Stramma and Schott* [1999] (their Figure 4): waters from the west (the NECC) and from the northwest (the Canary Current: CC) penetrate into the Gulf of Guinea along 4°N. The preferred pathway of the GUC along 4°N from Cape Palmas to Cape Three Points effectively follows the GC pathway, at deeper depth. However, the seasonal variability of the GC velocity (minimum in winter and maximum in summer), affected by the seasonal variability of both the NECC and CC, is different than the seasonal variability of the GUC.

On the other hand, it would be interesting to further investigate the role of the GUC on the mixing of the water masses and the impact of tropical and coastal waves.

Acknowledgments

The research leading to these results received funding from the EU FP7/2007-2013 under grant agreement 603521, PREFACE. We want to acknowledge all those who contributed to the PIRATA network maintenance and data processing and to the vessels 'officers and crews. We do thank Bruno Blanke and Nicolas Grima for their help on ARIANE Lagrangian tool, as well as Gildas Cambon for his help and participation on the implementation of ROMS simulations. We also acknowledge Cyrille Akuetevi and Frédéric Bonou, who initiated part of the descriptive works presented in this paper during their Master 2 training periods at the International Chair UNESCO of Mathematical Physics and Applications (ICMPA) of University Abomey-Calavi in Cotonou (Benin). The set of PIRATA cruises used in this study are available through: http://campagnes.flotteoceanographique.fr/series/14/ under collection name "PIRATA" (DOI:http://dx.doi.org/10.18142/14). The PIRATA processed SADCP data from 2007 to 2016 are available through: http://seanoe.org/data/00335/44635/under collection name "French PIRATA cruises: S-ADCP data" (DOI: http://dx.doi.org/10.17882/44635).

References

Arhan, M., H. Mercier, Y. Gouriou, and B. Bourlès (1998), Hydrographic sections across the Atlantic Ocean at 7°30′N and 4°30′S, *Deep Sea Res., Part I*, *45*, 829–872.

Arnault, S. (1987), Tropical Atlantic geostrophic currents and ship drifts, *J. Geophys. Res.*, *92*(C5), 5076–5088.

Bakun, A. (1978), Guinea current upwelling, *Nature*, *271*, 147–150.

Blanke, B., and S. Raynaud (1997), Kinematics of the Pacific equatorial undercurrent: An Eulerian and Lagrangian approach from GCM results, *J. Phys. Oceanogr.*, *27*(6), 1038–1053.

Blanke, B., M. Arhan, G. Madec, and S. Roche (1999), Warm water paths in the equatorial Atlanticas diagnosed with a general circulation model, *J. Phys. Oceanogr.*, *29*, 2753–2768.

Bourlès, B., D'Orgeville, M., G. Eldin, Y. Gouriou, R. Chuchla, Y. DuPenhoat, and S. Arnault (2002), On the evolution of the thermocline and subthermocline eastward currents in the equatorial Atlantic, *Geophys. Res. Lett.*, *29*(16), 1785, doi:10.1029/2002GL015098.

Bourlès, B., P. Brandt, G. Caniaux, M. Dengler, Y. Gouriou, E. Key, R. Lumpkin, F. Marin, R. L. Molinari, and C. Schmid (2007), African Monsoon Multidisciplinary Analysis (AMMA): Special measurements in the Tropical Atlantic, *CLIVAR Exch. Lett.*, *41*, 12–2.

Bourlès, B., et al. (2008), PIRATA program: History, accomplishments and future directions, *Bull. Am. Meteorol. Soc.*, *89*(8), 1111–1125, doi:10.1175/2008BAMS2462.1.

Brandt, P., G. Caniaux, B. Bourlès, A. Lazar, M. Dengler, A. Funk, V. Hormann, H. Giordani, and F. Marin (2011), Equatorial upper-ocean dynamics and their interaction with the West African monsoon, *Atmos. Sci. Lett.*, *12*(1), 24–30, doi:10.1002/asl.287.

Caniaux G., H. Giordani, J.-L. Redelsperger, F. Guichard, E. Key, and M. Wade (2011), Coupling between the Atlantic cold tongue and the West African monsoon in boreal spring and summer, *J. Geophys. Res.*, *116*, C04003, doi:10.1029/2010JC006570.

Chelton, D. B., R. A. deSzoeke, M. G. Schlax, K. E. Naggar, and N. Siwertz (1998), Geographical variability of the first-baroclinic Rossby radius of deformation, *J. Phys. Oceanogr.*, *28*, 433–460.

Colin, C. (1988), upwelling events in front of the Ivory Coast during the FOCAL program, *Oceanol. Acta*, *1*(1), 125–138.

Dai, A., and K. E. Trenberth (2002), Estimates of freshwater discharge from continents: Latitudinal and seasonal variations, *J. Hydrometeorol.*, *3*, 660–687.

Da Silva, A.M., C. C. Young, and S. Levitus (1994), Atlas of surface marine data 1994, Algorithms and Procedures, Vol. 1, NOAA (National Oceanic & Atmospheric Administration) Atlas NESDIS (National Environmental Satellite, Data, and Information Service), *6*, 83pp.

Debreu, L., P. Marchesiello, P. Penven, and G. Cambon (2012), Two-way nesting in split-explicit ocean models: Algorithms, implementation and validation, *Ocean Modell.*, *49-50*, 1–21.

Djakouré, S., P. Penven, B. Bourlès, J. Veitch, and V. Koné (2014), Coastally trapped eddies in the north of the Gulf of Guinea, *J. Geophys. Res. Oceans*, *119*, 6805–6819, doi:10.1002/2014JC010243.

Djakouré, S., P. Penven, B. Bourlès, and V. Koné (2016) Inertial terms effects on the ocean dynamics in the Gulf of Guinea, in revision for Geophysical Research-Oceans.

Donguy, J. R., and M. Privé (1964), Les conditions de l'Atlantique entre Abidjan et l'équateur. Deuxième partie. Variations hydrologiques annuelles, *Cah. ORSTOM, Sér. Oceanogr., XVI*, *3*, 193–204.

Elmoussaoui, A., M. Arhan, and A.-M. Treguier (2005), Model-inferred upper ocean circulation in the eastern tropics of the North Atlantic, *Deep Sea Res., Part I*, *52*(7), 1093–1120, doi:10.1016/j.dsr.2005.01.010.

Gouriou, Y. and G. Reverdin (1992), Isopycnal and diapycnal circulation of the upper equatorial Atlantic Ocean in 1983-1984, *J. Geophys. Res.*, *97*(C3), 3543–3572.

Haidvogel, D., and A. Beckmann (1999), *Numerical Ocean Circulation Modeling, Ser. Environ. Sci. Manage.*, vol. 2, 318 pp., Imperial College Press, London.

Hazeleger, W., and P. de Vries (2003), Fate of the Equatorial Undercurrent in the Atlantic, in *Interhemispheric Water Exchange in the Atlantic Ocean*, edited by G. J. Goni and P. Malamotte-Rizzoli, pp. 175–191, Elsevier Oceanographic Series.

Herbert, G., C. Kermabon, J. Grelet, and B. Bourlès (2015), French PIRATA cruises S-ADCP data processing, *Mercator Ocean Q. Newsl.*, *2015-05*(52), 22–26.

Hisard, P., and C. Hénin (1987), Response of the equatorial Atlantic Ocean to the 1983-1984 wind from the Programme Français Océan et Climat dans l'Atlantique équatorial cruise dataset, *J. Geophys. Res.*, *92*(C4), 3759–3768.

Hisard, P., and J. Merle (1979), Onset of surface summer cooling in the Gulf of Guinea during GATE, *Deep Sea Res.*, Part A, 26(GATE suppl. II), 325-342.

Hisard, P., J. Citeau, and A. Morlière (1976), Le système des contre-courants équatoriaux subsuperficiels, permanence et extension de la branche sud dans l'Océan Atlantique. *Cahiers Off. Rech. Sci. Tech. Outre-Mer, Sér. Océanogr.*, *14*, 209–220.

Kolodziejczyk, N., B. Bourlès, F. Marin, J. Grelet, and R. Chuchla (2009), Seasonal variability of the Equatorial Undercurrent at 10°W as inferred from recent in situ observations, *J. Geophys. Res.*, *114*, C06014, doi:10.1029/2008JC004976.

Kolodziejczyk, N., F. Marin, B. Bourlès, Y. Gouriou, *and* H. Berger *(*2014), Seasonal variability of the equatorial undercurrent termination and associated salinity maximum in the Gulf of Guinea, *Clim. Dyn.*, *43*(11*)*, 3025–3046, doi:10.1007/s00382-014-2107-7.

Leduc-Leballeur, M., G. de Coetlogon, and L. Eymard (2013), Air – sea interaction in the Gulf of Guinea at intraseasonal time-scales: Wind bursts and coastal precipitation in boreal spring, *Q. J. R. Meteorol. Soc.*, *139*, 387–400, doi:10.1002/qj.1981.

Lemasson, L., and J.-P. Rebert (1968), Observations de courants sur le plateau continental ivoirien: Mise en évidence d'un sous-courant, *Doc. Sci. Prov. Cent. Rech. Océanogr. Abidjan*, *22*, 66.

Lemasson, L., and J.-P. Rebert (1973a), Circulation dans la partie orientale de l'Atlantique Sud, *Doc. Sci. Cent. Rech. Océanogr. Abidjan*, *IV*(1), 91–124.

Lemasson, L., and J.-P. Rebert (1973b), Les courants marins dans le Golfe Ivoirien, *Cah. ORS TOM, Sér. Océanogr.*, *11*(1), 67–95.

Lumpkin, R. and S. L. Garzoli (2005), Near-surface circulation in the tropical Atlantic Ocean, *Deep-Sea Res., Part I*, *52*(3), 495–518, doi: 10.1016/j.dsr.2004.09.001.

Marchal, E., and J. Picaut (1977), Répartition et abondance évaluées par écho-intégration des poissons du plateau ivoiro-ghanéen en relation avec les upwellings locaux, *J. Rech. Océanogr.*, *II*(4), 39–57.

Marin, F., G. Caniaux, B. Bourlès, H. Giordani, Y. Gouriou, and E. Key (2009), Why were sea surface temperatures so different in the Eastern Equatorial Atlantic in June 2005 and 2006, *J. Phys. Oceanogr.*, *39*, 1416–1431, doi:10.1175/2008JPO4030.1.

Mercier, H., M. Arhan, and J.R.E. Lutjeharms (2003), Upper-layer circulation in the eastern Equatorial and South Atlantic Ocean in January-March 1995, *Deep Sea Res., Part I*, *50*(7), 863–887.

Morlière, A. (1970), Les saisons marines devant Abidjan, *Doc. Sci. Cent. Rech. Océanogr.*, *1*(2), 1–15.

Penven, P., P. Marchesiello, L. Debreu, and J. Lefevre (2008), Software tools for pre- and post-processing of oceanic regional simulations, *Environ. Modell. Software*, *23*, 2008 660–662.

Picaut, J. (1983), Propagation of the seasonal upwelling in the eastern equatorial Atlantic, *J. Phys. Oceanogr.*, *13*, 18–37.

Piton, B., and S. Wacongne (1985), Unusual amounts of very saline subsurface water in the Eastern gulf of Guinea in May 1984, *Trop. Ocean Atmos. Newsl.*, *32*, 5–8.

Redelsperger, J. L., C. Thorncroft, A. Diedhiou, T. Lebel, D. Parker and J. Polcher (2006), African Monsoon Multidisciplinary Analysis: An international project and field campaign, *Bull. Am. Meteorol. Soc.*, *87*(12), 1739–1746, doi:10.1175/BAMS-87-12-1739.

Roy, C. (1995), The Côte d'Ivoire and Ghana Coastal Upwellings: Dynamics and Changes, in acts of DUSRU (Dynamics and Use of Sardinella Resources From Upwelling off Ghana and Ivory Coast) meeting, edited by F. X. Bard and K. A. Koranteng, pp: 346–361, ORSTOM (Office de la Recherche Scientifique et Technique Outre Mer), Paris.

Schott, F., J. McCreary, and G. Johnson (2004), Shallow overturning circulations of the tropical subtropical oceans, in *Earth Climate: The Ocean-Atmosphere Interaction, AGU Geophys. Monogr. Ser.*, 147, edited by C. Wang, S.-P. Xie, and J. A. Carton, pp. 261–304, AGU, Washington, D. C.

Servain, J., J. Picaut, and J. Merle (1982), Evidence of remote forcing in the equatorial Atlantic Ocean, *J. Phys. Oceanogr.*, *12*, 457–463.

Shchepetkin, A. F., and J.-C. McWilliams (2005), The Regional Ocean Modeling System: A split-explicit, free-surface, topography following coordinates ocean model, *Ocean Modell.*, *9*, 347–404.

Stramma, L., and F. A. Schott (1999), The mean flow field of the tropical Atlantic Ocean, *Deep Sea Res., Part II*, *46* (29), 279 – 303.

Tsuchiya, M. (1986), Thermostats and circulation in the upper layer of the Atlantic Ocean, *Prog. Oceanogr.*, *16*, 235–267.

Verstraete, J.-M. (1992), The seasonal upwellings in the Gulf of Guinea, *Prog. Oceanogr.*, *29*, 1–60.